National Library of Canada

Acquisitions and Bibliographic Services Branch

395 Wellington Street
Ottawa, Ontario
K1A 0N4

Bibliothèque nationale du Canada

Direction des acquisitions et des services bibliographiques

395, rue Wellington
Ottawa (Ontario)
K1A 0N4

Your file Votre référence

Our file Notre référence

NOTICE

The quality of this microform is heavily dependent upon the quality of the original thesis submitted for microfilming. Every effort has been made to ensure the highest quality of reproduction possible.

If pages are missing, contact the university which granted the degree.

Some pages may have indistinct print especially if the original pages were typed with a poor typewriter ribbon or if the university sent us an inferior photocopy.

AVIS

La qualité de cette microforme dépend grandement de la qualité de la thèse soumise au microfilmage. Nous avons tout fait pour assurer une qualité supérieure de reproduction.

S'il manque des pages, veuillez communiquer avec l'université qui a conféré le grade.

La qualité d'impression de certaines pages peut laisser à désirer, surtout si les pages originales ont été dactylographiées à l'aide d'un ruban usé ou si l'université nous a fait parvenir une photocopie de qualité inférieure.

Canada

OPTICAL CDMA SYSTEM BASED ON SPECTRAL AMPLITUDE ENCODING OF INCOHERENT BROADBAND SOURCES

by

Lucie Adam, B.Ing.

A thesis submitted to the
School of Graduate Studies and Research
in partial fulfillment of the requirements for the degree of

Master of Applied Science

Ottawa-Carleton Institute for Electrical Engineering

Department of Electrical Engineering
Faculty of Engineering
University of Ottawa

December 1995

ISBN 0-612-11533-X

Canada

UNIVERSITÉ D'OTTAWA
UNIVERSITY OF OTTAWA

Abstract

In this thesis, a new optical Code-Division-Multiple Access (CDMA) system is demonstrated based on spectral amplitude encoding of noncoherent broadband sources. This scheme employs low-cost optical sources such as light-emitting diodes (LEDs). The spreading gain is independent of the data rate, therefore individual users can operate at data rates compatible with available electronic devices.

Optical CDMA systems are generally classified into two categories: time-encoded and frequency-encoded systems. In the former case, a low information rate is mapped into a high rate optical pulse sequence. This is possible because of the wide bandwidth of optical fibers. The latter relies on encoding the entire available wavelength band at once with a sequence identifying the intended user.

The encoding and decoding principles rely solely upon the crosscorrelation properties exhibited by the set of signals used to distinguish subscribers. We employ simple maximal-length sequences. We demonstrate how data is recovered or rejected with the use of a differential receiver. We examine the transceiver design, and the impact of their characteristics on the system capacity.

The performance of the proposed CDMA system is experimentally characterized. The experimental set-up and its advantages and limitations are detailed. We present our bit-error rate (BER) measurements for different code lengths and received power. Also, the resulting eye patterns are shown.

Acknowledgments

I would like to express my sincere gratitude to my thesis supervisor, Dr. Mohsen Kavehrad who has been very supportive of this work. His guidance and helpfulness are greatly appreciated. Also, thanks to Dr. Quan Jiang for his guidance on electronics. My most sincere gratitude goes to Dr. Eli Simova, for numerous hours of experimentation and discussion.

This work was supported in parts by the Telecommunications Research Institute of Ontario (TRIO), Photonics Networks and Systems Thrust and by the Natural Sciences and Engineering Research Council of Canada (NSERC). I am grateful to both of these organizations.

Also, many thanks to my colleagues at the Broadband Communications Research Laboratory of the University of Ottawa, for many useful discussions I had with them during the course of this work. Finally, many thanks to my family and friends, for their constant support and encouragement.

Table of Contents

List of Tables and Figures vi

List of Abbreviations viii

Chapter 1 Introduction 1
1.1 Motivations 1
1.2 Contributions and Outline of the Thesis 3

Chapter 2 A Brief Overview of Optical CDMA Systems 5
2.1 Introduction 5
2.2 Time-Encoded Systems 6
2.2.1 Incoherent Time Domain Encoding 7
2.2.2 Coherent Time Domain Encoding 8
2.3 Frequency-Encoded Systems 9
2.3.1 Phase Encoding or Spread-Time Systems 10
2.3.2 Amplitude Encoding 10
2.3.3 Spectral Slicing 13
2.4 Hybrid Systems 14
2.4.1 Time/Space 14
2.4.2 Time/Wavelength 15

Chapter 3 Amplitude Encoded Optical CDMA System 17
3.1 Principle of Operation 17
3.1.1 M-Sequences 18
3.1.2 Hadamard Codes 19
3.2 Transceivers Design 20
3.2.1 Encoding in the Frequency Domain 20
3.2.2 Coherent and Noncoherent Coding 22
3.2.3 Proposed Transmitter 25
3.2.4 Decoding Procedure 27
3.2.5 Proposed Receiver 31
3.2.6 Receiver Electronics 32
3.3 Optical Parameters of Transceivers and Their Impact on System Capacity 33
3.3.1 Diffraction-Limited Performance 33
3.3.2 The Spectroscopic Instrument 37
3.3.3 Ray Tracing 40
3.4 Practical Considerations for System Implementation 44
3.4.1 Amplitude Masks 44
3.4.2 Spectral Shape of the LED 44

Chapter 4 An Experiment on the Proposed System 46
4.1 Experimental Set-up 46
4.2 Bit-Error Rate Performance 48
4.2.1 7 Chip Mask 48
4.2.2 15 Chip Mask 51
4.3 BER vs Received Power 53
4.4 Power Budget 55

Chapter 5 Concluding Remarks and Suggestions for Future Study ... 58

Appendix 64

References 68

List of Tables and Figures

Tables

		page
4.1	Theoretical and Experimental Optical Power Losses in the proposed system.	56

Figures

		page
2.1	A schematic diagram of a general optical CDMA system.	5
2.2	Time domain CDMA using unipolar codes (0,1).	6
2.3	Incoherent time domain coding schemes.	7
2.4	Hybrid Temporal/Spatial optical CDMA network.	15
2.5	Hybrid wavelength hopping/time spreading CDMA network.	15
3.1	Spectral slicing.	21
3.2	LED spectrum filtering with an amplitude mask.	21
3.3	Schematic Diagram of the encoding set-up.	22
3.4	Littrow mounting.	26
3.5	Proposed transmitter.	26
3.6	Modification to the proposed transmitter.	27
3.7	Schematic diagram of the receiver.	28
3.8	Decoding principle.	30
3.9	Proposed receiver.	31
3.10	Electronic circuit for signal recovery.	32
3.11	(a) Bessel function of the first kind. (b) Two-dimensional Fraunhofer diffraction pattern by a circular aperture.	34
3.12	(a) Numerical aperture of fiber. (b) Entrance pupil of system.	35

		page
3.13	Spectral resolution.	35
3.14	Spot diagrams.	41
3.15	Cumulative Radial Power distribution at the output focal plane of the transmitter.	41
3.16	Geometrical ray tracing plots for the transmitter and the receiver.	43
4.1	Schematic diagram of the set-up used for the optical CDMA amplitude encoding experiment.	46
4.2	Spectrum as encoded by a 7 chip mask.	49
4.3	Eye pattern measurements obtained with a 7 chip code.	50
4.4	Testing of the processing gain.	50
4.5	Spectrum as encoded by a 15 chip mask.	51
4.6	Eye pattern measurements obtained with a 15 chip code.	52
4.7	Electrical parameters appearing in the computation of P_o.	53
4.8	Curve of Bit-Error Rate measurements as a function of Mean Optical Power detected in the arm with the matching mask.	54

List of Abbreviations

AlGaAs	Aluminum Gallium Arsenide
ASE	Amplified Spontaneous Emission
ATM	Asynchronous Transfer Mode
BER	Bit-Error Rate
CDMA	Code-Division-Multiple Access
EDFA	Erbium-Doped Fiber Amplifier
IR	Infra-Red
LAN	Local-Area Network
LED	Light-Emitting Diode
NA	Numerical Aperture
OOC	Optical Orthogonal Code
PD1	Photodetector #1
PD2	Photodetector #2
p-i-n	Describes the basic structure of the junction. Intrinsic layer in between the p- and n- contacts
RF	Radio Frequency
SLD	Superluminescent Diode
SLM	Spatial Light Modulator
SNR	Signal-to-Noise Ratio
TIR	Total Internal Reflection
TDM	Time Division Multiplexing
TTL	Transistor Transistor Logic
WDM	Wavelength Division Multiplexing

Chapter 1

Introduction

1.1 Motivations

The first low-loss optical fiber suitable for telecommunications use was reported in the early 1970s [1]. During the following years, rapid advances in lightwave technology and continually increasing demand for cost-effective transmission of information have propelled optical fiber communication systems from a research stage to a wide commercial deployment, over the continents and across the oceans. With the large bandwidth available on fiber optic channels, it is possible to offer subscribers a wide array of telecommunication services, including voice, data, facsimile, and video. The recent arrival of erbium-doped fiber amplifiers (EDFAs) [2] has now attracted world-wide attention for long-distance communications. In our present information age, lightwave technology has a bright future indeed.

Nonetheless, for optical communications and networking applications, the problems to solve are numerous. For example, realizing a photonic network requires an efficient multiple-access technique. In North America, research concentrates mainly on Wavelength Division Multiplexing (WDM). This technique allows an easy tapping of the large bandwidth available in optical fibers. However, stable lasers with precise wavelength control or with large tuning capability are required, as well as narrowband optical bandpass filters at the receiver.

Another multiple-access technique relies on dividing time into slots and assigning them to subscribers. Nowadays, the Time Division Multiplexing (TDM) access technique is widely used in electronics world for its simplicity. A major drawback of this scheme comes from the need for precise synchronization between the users within a network. Moreover, in a bursty traffic network, use of available bandwidth is highly inefficient since only a small fraction of the users would typically transmit at the same time.

In a Code Division Multiple Access (CDMA) system, the access capability is attributed to coding. A minimally interfering address code is assigned to each subscriber information bits in a network. It can provide asynchronous multiplexing for high-speed networks. It allows many sources to operate independently on the same channel, with a minimum amount of interference. The maximum number of subscribers is however limited by the number of codes in a given set. Also, in conventional time-domain CDMA, each bit of the input signal is encoded into a waveform that corresponds to the destination address of the data, so that the real bit rate is multiplied proportional to the code length. As information rates increase, limited speed of optoelectronic devices becomes a serious problem.

In an attempt to overcome this obstacle, new types of optical networks have emerged based on passive optical signal processing, including optical CDMA networks. In these systems, a single source provides the necessary wavelength range and the encoding is performed by modulating the entire available wavelength band at once. Individual users can thus operate at data rates compatible with available electronic modulation and processing circuits, making this scheme more practical than time-domain CDMA.

In this thesis, we present the results of a proof-of-concept demonstration of an optical CDMA system, based on spectral amplitude encoding of spectrally sliced incoherent broadband sources [3-5]. This scheme requires standard optical elements, simple direct-detection receivers and low-cost sources such as light-emitting diodes (LEDs) and superluminescent diodes (SLDs).

1.2 Contributions and Outline of the Thesis

To the best of our knowledge, this work constitutes the first complete experimental demonstration of an optical CDMA communication system based on amplitude encoding of a noncoherent source. This was the first time data was encoded and recovered using this particular method experimentally. The proof-of-concept is undoubtedly the most important contribution of this thesis.

In Chapter 2, a brief summary of different optical CDMA systems in literature is presented. The systems are categorized according to the type of encoding/decoding performed (coherent or incoherent), and the encoding domain (time, frequency or space).

Chapter 3 focuses on the proposed optical CDMA system. First, the principle of operation is explained. As address codes, we use simple maximum-length sequences also known as m-sequences. We detail how data is recovered or rejected using a differential receiver. We consider the architecture requirements for the transceivers. We were the first to recognize that the theory of Fourier optics was not necessary to explain the system principle of operation, since the encoding is performed on amplitude rather than on phase. With this fact in mind, we propose a different configuration for the encoder and decoder, more compact than what was originally suggested [3]. This compact configuration is one of the major contributions of the thesis. Another important contribution lies in the simplification of the differential receiver design. We conclude this chapter with a look at some practical considerations for optical transceiver design. We see how these parameters affect the system capacity.

Experimental results are presented in Chapter 4. We describe in detail the experimental set-up. We present spectra encoded by masks of different lengths. We discuss the effect of the code length on the system performance. Bit error rate tests are reported. We present a measured bit error rate curve as a function of received power for one user. The results are promising. Part of the work presented in Chapters 3 and 4 has been presented in [6]. Finally, in Chapter 5, we give a summary of results and suggestions for future work.

Chapter 2

A Brief Overview of Optical CDMA Systems

2.1 Introduction

In a CDMA system, the multi-access capability is attributed to coding. An address code is assigned to each subscriber in the network. It can provide asynchronous multiplexing for high-speed networks, eliminating the need to maintain synchronism throughout the network, as in the case with TDM. It allows many sources to operate independently on the same channel, with a minimum amount of interference. The maximum number of subscribers is limited by the number of codes in a given set. A block diagram of an optical CDMA system is presented in Fig. 2.1. The N inputs to the $N \times N$ star coupler come from the N different encoders of each user. The N outputs go to N decoding modules, with a different code assigned to each.

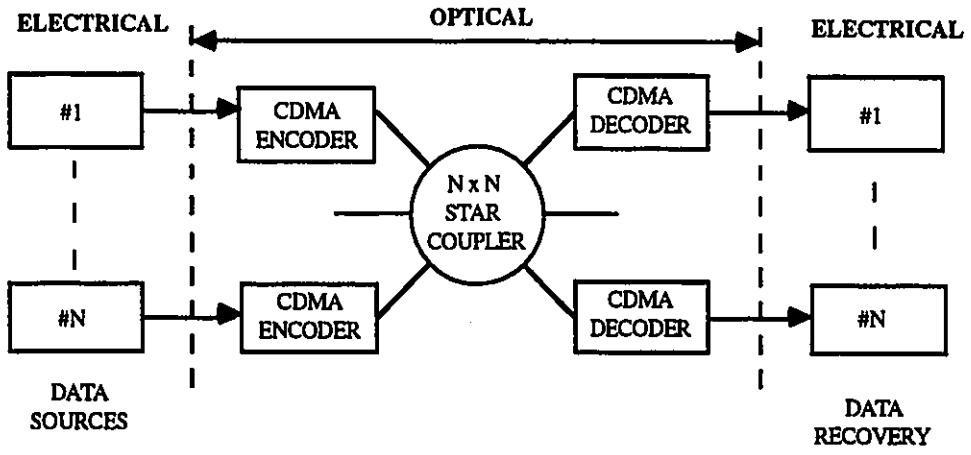

Fig. 2.1 A schematic diagram of a general optical CDMA system.

In this chapter we review some of the different types of optical CDMA systems. A system classification is made according to the domain where the encoding is performed, i.e., time, space or frequency, and according to the type of encoding/decoding performed, be it coherent or incoherent. We present the advantages and drawbacks of each approach [7,8].

2.2 Time-Encoded Systems

In time-encoded CDMA systems, the asynchronous multiple access is achieved by mapping a relatively low data rate signal into a high rate optical pulse sequence, made possible by the large bandwidth of optical fibers. Each bit of the input signal is transformed into a waveform which corresponds to the destination address of the data. The signal spectrum after encoding is broadened by a so-called spreading factor S. Fig. 2.2 illustrates the principle for a unipolar code word (0,1).

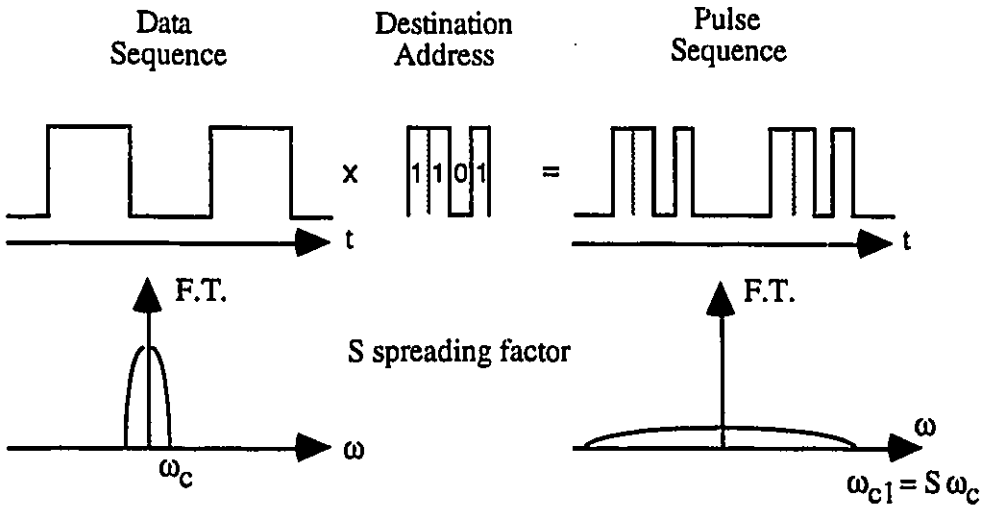

Fig. 2.2 Time domain CDMA using unipolar codes (0,1).

2.2.1 Incoherent Time Domain Encoding

Time-encoded CDMA systems can be classified according to the type of decoding process performed, coherent or incoherent. For incoherent processing, the correlation at the receiver is based on light intensity rather than on field superposition. Therefore, incoherent systems use direct detection receivers. They operate to detect the instantaneous optical power as it arrives at the receiver. Such receivers exhibit the simplest type of implementation.

In general, bipolar codes (-1,+1) cannot be used with incoherent processing, since the same power is associated with a -1 and a +1. New unipolar codes (0,1) had to be designed, such as prime codes, optical orthogonal codes (OOC) [9] and quadratic congruence codes [10]. The data encoding can be performed simply by using a short optical pulse and optical delay lines that consist of a $1 \times w$ power splitter, w parallel delay lines and a $w \times 1$ combiner, w being the code weight (number of 1's). The encoder is shown in Fig. 2.3(a). The number of delay lines should be small in order to reduce the complexity and recombining losses, which are proportional to $10 \log N$. In a different approach, 3 dB couplers are cascaded, leading to a total loss of 6 dB, regardless of the code weight and length (Fig. 2.3(b)). Incoherent time-domain CDMA systems have received the most attention in research so far, including the work of Prucnal et al., Petrovic and Holmes, Salehi and Brackett, and Kwong [11-16].

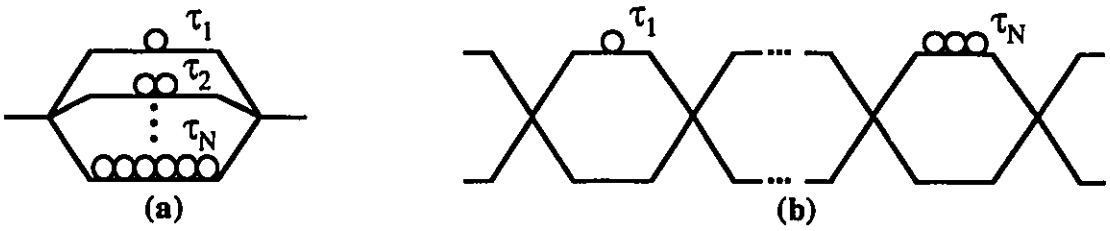

Fig. 2.3 Incoherent time domain coding schemes. **(a)** Tapped delay lines. **(b)** Ladder Networks.

Recently, Nguyen, Aazhang and Young presented a method for transmission and detection of bipolar sequences in a unipolar system [17]. This will allow implementation of bipolar codes with direct detection receivers.

Advantages of incoherent CDMA include simplicity of transceiver design, simple direct detection receivers, generally low-cost optical sources because incoherent encoding does not require sources with long coherence time. Also, compared to WDM, there is no need for precise carrier frequency stabilization and for narrowband optical filters. The stability requirements for the processing elements are small and need only to be in the order of the chip period when using delay lines. The main disadvantage is the reduced number of codes in a particular set. More details can be found in [9]. Reconfiguration of the transmitter requires changing the values of the delays. This remains a technological challenge.

2.2.2 Coherent Time Domain Encoding

Coherent detection relies on field superposition, exploiting the waveform nature of light; it is polarization dependent. Two categories of coherent systems are found, depending on whether or not they use a local oscillator at the receiver. A receiver having a local oscillator is a heterodyning receiver. A locally generated lightwave field is optically mixed with the received field, and the combined waveform is photodetected. Such receivers are used whenever information is amplitude modulated, frequency modulated, or phase modulated onto the optical carrier. Heterodyning receivers are more difficult to implement than direct detection receivers and require close matching of the spatial patterns of the two optical fields being mixed, i.e., matching of their polarizations.

With a local oscillator, bipolar codes can be used and the correlation can be done in the electronics domain. The detection level for the desired user is maximized, because of coherency. This allows shorter sequence lengths than in purely incoherent systems. Also, a larger number of users can be accommodated. However, these systems require precise

frequency tuning, polarization matching between the incoming signal and the local oscillator, phase control and a low phase noise. Transmitter reconfigurability is also a problem [18].

Coherent optical CDMA using low-coherence sources can also be found in the literature [19-21]. It includes the work of Sampson, Jackson, Griffin, Marhic and Chang. The encoding/decoding can be done all optically with a ladder network, similar to the one shown in Fig. 2.3(b). A necessary condition for coherent correlation to take place is that the receiver delays match those at the transmitter to within the coherence time of the source. This is typically less than 1 ps and therefore requires complex electronics, such as control loops in order to compensate the change in the optical path lengths induced by temperature variations [21]. Very precise control of delays in the coding architecture is therefore needed. Code design for this system is only at an early stage.

However, all time-encoded systems suffer from the same limitation. As the number of simultaneous subscribers increases, so does the code length, resulting in a spectrum broadening that would translate into an extremely high rate optical pulse sequence. As information rates increase, limited speed of optoelectronic devices becomes a serious problem.

2.3 Frequency-Encoded Systems

In an attempt to overcome the limited speed obstacle encountered with time-encoded CDMA, new types of optical networks have emerged based on passive optical signal processing. In these frequency-encoded systems, the addressing is performed by encoding the entire available wavelength band at once with the sequence corresponding to the intended user. Individual users can thus operate at data rates compatible with available electronics, making this scheme more practical than time-domain CDMA.

2.3.1 Phase Encoding or Spread-Time Systems

Spread-time systems were first proposed by Weiner, et al. [22]. They are based on coherent encoding of ultrashort light pulses. The technique consists of encoding the phase of the different spectral components contained within ultrashort optical pulses. These pulses impinge on a grating and lens apparatus, which spatially disperse the spectral components of the pulse. A spatially patterned mask scrambles the spectral phases. A second lens and grating recombine all the frequency components into a single collimated beam which now contains the destination address code of the data. The decoder consists of a second apparatus similar to the encoder with a phase mask equal and opposite to that in the corresponding encoder. For matched encoders and decoders, the total added spectral phase is zero, and the original ultrashort pulse is restored. For sufficiently different masks, the spectral phases in the decoder are rearranged but not canceled. The decoded signal remains a low intensity noise burst below the threshold level. The system is described in more details in the next chapter. Because of optical signal processing, spread-time systems allow data rates a lot higher than time-encoded systems. However, ultrashort pulses are generated with expensive mode-locked lasers. Any type of dispersion also limits the achievable transmission distance [23].

2.3.2 Amplitude Encoding

This scheme was first proposed in [3]. This optical CDMA system is based on encoding the spectrum of noncoherent broadband sources, via an amplitude mask. The scheme requires standard optical elements, simple direct detection receivers and low-cost sources such as light-emitting diodes (LEDs) or superluminescent diodes (SLDs). The aim of this thesis is to experimentally demonstrate the feasibility of the present system. The first complete proof-of-concept experiment was presented in [6], using a near-Littrow configuration for the gratings. A theoretical review will be presented in the next chapter.

A different approach was proposed by Iversen et al. [24], where the wavelength filtering is provided by acousto-optic tunable filters, avoiding the use of lenses, gratings and amplitude masks to encode and decode the broadband spectrum. However, with technologies currently available, it is very difficult to control the passband of acousto-optic filters. Besides, the extinction ratio achieved by these is very small compared to amplitude masks. Amplitude encoding was adopted for two dimensional image transmission by Kitayama. System description is found in [25].

Modifying the encoding scheme originally proposed by Zaccarin and Kavehrad, Su and Chen demonstrated an increase of the access capacity from N to $N^2/4$, where N is the number of frequency bands resolved by the encoder [26]. They proposed an encoding scheme using double m-sequences on the mask, and four photodetectors to collect the light instead of two.

CDMA amplitude encoding with LEDs is limited to Local-Area Network (LAN) applications because optical signals become increasingly distorted as they travel along a fiber. This distortion is a consequence of intramodal dispersion and intermodal delay effects. The distortion effects can be explained by examining the behavior of the group velocities of the guided modes, where the group velocity is the speed at which energy in a particular mode travels along the fiber.

In a multi-mode fiber system, material dispersion and intermodal delay limit the transmission length to under 10 km at a modulation rate of 32 Mbps [27]. Material dispersion arises from the variation of the refractive index of the core material as a function of wavelength. This causes a wavelength dependence of the group velocity of any given mode. Pulse spreading occurs even if the different wavelengths follow the same path. This problem is extremely severe when using optical sources with broad spectral width, such as LEDs. The pulse spread σ_{mat} for a source of spectral width σ_λ is given by [28]:

$$\sigma_{mat} = -\frac{L}{c}\lambda\frac{d^2n}{d\lambda^2}\sigma_\lambda = D_{mat}(\lambda)L\sigma_\lambda \qquad (2.1)$$

where L is the distance traveled by the pulse in kilometers, c is the speed of light in free space, λ is the nominal wavelength of the source in nm, $n = n(\lambda)$ the core refractive index, and $D_{mat}(\lambda)$ is the material dispersion in ps/(nm·km). As an example, a typical GaAlAs LED having a spectral width of 40 nm at a 800 nm nominal wavelength produces a pulse spread of 4.4 ns/km. For a modulation rate of 100 Mbps, two consecutive pulses will overlap after a traveled distance of ≈2.2 km. This distance is reduced to 0.5 km for a modulation rate of 500 Mbps. These modulation rates are the best a high performance LED can achieve.

For multi-mode fibers, the most severe problem arises from intermodal delay. It is a result from mode having a different value of the group velocity at a single frequency. It depends on the fiber characteristics and is therefore independent of the type of source used. The modal dispersion is given by [28]:

$$t_{mod} = \frac{0.44}{B_M} = \frac{0.44 L^q}{B_0} \tag{2.2}$$

where B_M is the bandwidth in a link of length L, B_0 the bandwidth of a 1 km length of cable, and q is a parameter with a range between 0.5 and 1. A value of $q = 0.5$ indicates a steady-state modal equilibrium, and $q = 1$ indicates little mode mixing. From experience, a reasonable estimate is $q = 0.7$. The larger the core, the smaller the bandwidth-distance product. For the fiber used in the experiment (core diameter of 200 μm), the bandwidth-distance product is approximately 20 MHz-km. With these values, a modal dispersion of 22 ns is seen after a 1 km link. At 100 Mbps, two pulses will overlap after a propagation of 0.58 km. However, fibers with smaller cores can improve the propagation distance value.

Interference from different signals ("excess noise") in the network is a problem that appears in single-mode based systems [29]. The total light propagating through the network comes from many independent sources, but since combined in a single-mode fiber, interference will occur during the photodetection. This results in an optical beat noise of the same level as the intensity noise of one such source with the same optical power.

Since CDMA amplitude encoding is a power-limited system, it is not very suitable for single-mode systems where the coupling efficiency of a LED is much lower than for multi-mode fibers. For a fiber of core radius a and numerical aperture NA, the maximum theoretical coupling efficiency η_{max} is given by :

$$\eta_{max} = \begin{cases} \left(\frac{a}{r_s}\right)^2 (NA)^2 & \text{for } \frac{r_s}{a} > NA \\ 1 & \text{for } \frac{r_s}{a} \leq NA \end{cases} \tag{2.3}$$

where r_s is the radius of the emitting area [28]. For a multi-mode fiber of $NA = 0.2$ and 50 μm core diameter and an emitting area of 30 μm diameter, the coupling efficiency is 11%. For a similar emitting surface coupled to a single-mode fiber of $NA = 0.11$ and 8 μm core diameter, η_{max} drops to 0.1%.

2.3.3 Spectral Slicing

Even though these are WDM systems, spectral slicing techniques are presented in this chapter because of their similarities with spectral amplitude encoding systems. Both techniques are limited to local access and LAN applications because of the source power and incoherence nature, i.e., high coupling losses, material and multi-mode dispersion, limited modulation speed of LEDs. In WDM spectral slicing, the broad linewidth is divided into many channels with optical demultiplexers. Spectral slicing of LEDs has been demonstrated with a simple design of the transceivers [30]. Its operation is severely power-limited compared to the CDMA spectral amplitude encoding, because the latter technique uses the entire available spectral band at once. However, it does not suffer from intensity noise as severely as amplitude CDMA, since every user transmits over his own wavelength "slice," which will interfere only with neighboring slices used by other subscribers and not with the entire broadband available. Also, the routing relies on traditional WDM multiplexing/demultiplexing, therefore there are no splitting as in optical CDMA, using a broadcast star.

Other broad linewidth sources have been proposed for spectrally-sliced WDM systems such high-power amplified spontaneous emission (ASE) from EDFAs [31] and femtosecond sources [32]. The former is limited by the spontaneous-spontaneous beat noise. The latter require mode-locked lasers.

2.4 Hybrid Systems

Under this title are classified the systems where the encoding is performed in a combination of domains. So far, the research has mostly concentrated on two hybrid schemes: time/space and time/wavelength. These schemes allow higher bandwidth efficiency and network capacity than time-encoded CDMA systems.

2.4.1 Time/Space

Park, et al., [33] introduced a new noncoherent optical CDMA system, in which the encoding is performed in two dimensions : time and space. Each encoder consists of w optical delay lines as in Fig. 2.3, w being the weight of the code. A signal pulse is first encoded into a waveform corresponding to a code sequence. Each "1" of the code sequence is then redirected to one of the g $N \times N$ star couplers, where g is the code length and N the number of users. The system is shown in Fig. 2.4.

In contrast with one-dimensional time-encoded CDMA systems, the sequence length in each channel is reduced by a factor g. This results in a higher bandwidth efficiency. It is mentioned in [33] that ideally, an autocorrelation function without sidelobes can be theoretically obtained. However, this method has its drawbacks. Let's mention the need to exactly match the delays between the transmitters and receivers, and also the difficulty to work with g broadcast networks.

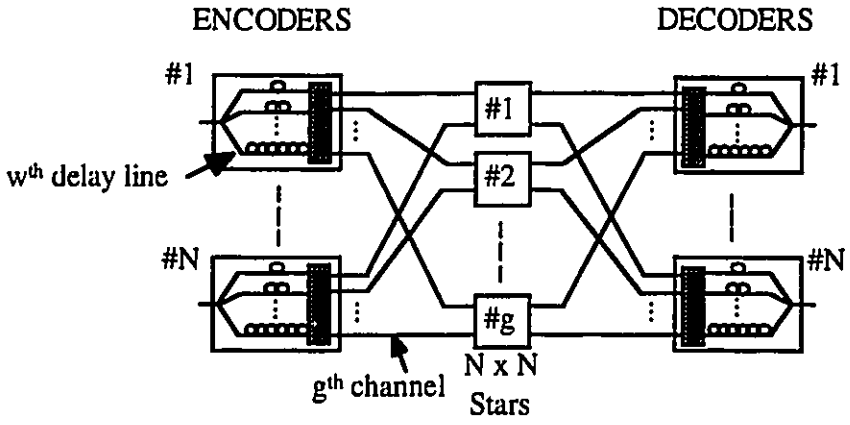

Fig. 2.4 Hybrid Temporal/Spatial optical CDMA network. Every "one" in the time spread pattern is transmitted by a different spatial channel (different star coupler). The optical interconnections in shaded areas depend on the code.

2.4.2 Time/Wavelength

Coding in time/wavelength dimensions is similar to time/space. In both schemes, the encoder consists of optical delay lines. However, in a time/wavelength system, different channels transmitting the 1's of the code sequence consist of different wavelengths, and not spatial channels. Therefore, this scheme increases the network capacity compared to a single-wavelength time-encoded system and a high level of privacy can be obtained. Good crosscorrelation and autocorrelation properties can also be obtained with pseudo-orthogonal codes [34,35].

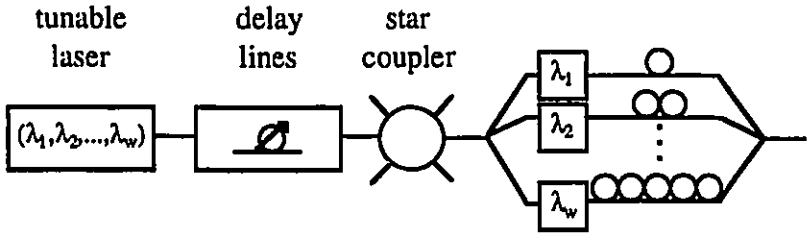

Fig. 2.5 Hybrid wavelength hopping/time spreading CDMA network. Each "one" in the time spread pattern is transmitted at a different wavelength.

This system has the same technological requirements as WDM systems, that is precise control over the wavelengths of the laser and the use of narrowband wavelength filters. At higher bit rates, the tuning time of the laser sources becomes a problem. Higher rates also require fast optical switches.

Chapter 3

Amplitude Encoded Optical CDMA System

In this chapter is presented the theory underlying optical CDMA based on spectral amplitude encoding of noncoherent sources. The principle of operation is first explained. The encoding and decoding procedures follow, as well as the proposed transceivers. Their optical characteristics and their impact on system capacity are investigated. We present the results of a geometrical ray tracing simulation. The chapter is concluded with some considerations for system implementation as a switch or network.

3.1 Principle of Operation

There are a large number of systems that require sets of signals in which each sequence in the set is easily distinguished from every other in the set. The sets of sequences employed are usually periodic, because of the implementation simplifications that arise from the use of the periodicity. In optical CDMA systems, the performance depends extensively on the crosscorrelation properties exhibited by the set of codes. For incoherent detection systems, such as amplitude encoded CDMA systems, unipolar codes (0,1) are required since the detection is based on accumulated received power.

Let $(\mathbf{X}) = (x_0, x_1, \cdots, x_{N-1})$ and $(\mathbf{Y}) = (y_0, y_1, \cdots, y_{N-1})$ be two sequences from a periodic code of length N. The periodic crosscorrelation of $(\mathbf{X})$ and $(\mathbf{Y})$ is:

$$\Theta_{XY}(k) = \sum_{i=0}^{N-1} x_i y_{i+k} \tag{3.1}$$

We define the complementary sequence of $(\mathbf{X})$ by $(\overline{\mathbf{X}})$, whose elements are obtained from $(\mathbf{X})$ by $\overline{x}_i = 1 - x_i$. The periodic crosscorrelation of $(\overline{\mathbf{X}})$ and $(\mathbf{Y})$ is:

$$\begin{aligned}\Theta_{\overline{X}Y}(k) &= \sum_{i=0}^{N-1} \overline{x}_i y_{i+k} = \sum_{i=0}^{N-1} (1 - x_i) y_{i+k} \\ &= \sum_{i=0}^{N-1} y_{i+k} - \Theta_{XY}(k)\end{aligned} \tag{3.2}$$

If the code used exhibits crosscorrelation properties such that

$$\Theta_{XY}(k) = \Theta_{\overline{X}Y}(k) \quad \text{for } k \neq 0, \tag{3.3}$$

then a receiver computing

$$Z = \Theta_{XY}(k) - \Theta_{\overline{X}Y}(k) \tag{3.4}$$

would reject any signal $(\mathbf{Y})^k$, with $k \neq 0$. Complete orthogonality between users would then be theoretically achieved by assigning the sequences of the code set to the subscribers of the network. Even though a user would receive all the signals sent through the network, the user would detect only its data. In the following subsections, we show two codes satisfying the condition $\Theta_{XY}(k) = \Theta_{\overline{X}Y}(k)$ [4].

3.1.1 M-Sequences

A class of signals with excellent crosscorrelation properties, are the maximal-length linear feedback shift register sequences, also known as m-sequences. Each sequence in a set is a cyclically shifted version of a single m-sequence; the sequences in the set are therefore periodic. In a unipolar m-sequence, the number of 1's and 0's always differ by one. In the following demonstration, we consider m-sequences of length N having $\frac{N-1}{2}$ 0's and $\frac{N+1}{2}$ 1's.

Let $(\mathbf{X})$ and $(\mathbf{Y})$ be two sequences from a set of unipolar m-sequences of length N. In that case, the sequence $(\mathbf{Y})$ is a cyclically shifted version of sequence $(\mathbf{X})$ and is

equal to $(\mathbf{Y}) = (\mathrm{T}^k\,\mathbf{X}) = (x_k, x_{k+1}, \cdots, x_{N-1}, x_0, \cdots, x_{k-1})$ where T is the operator that shifts vectors cyclically to the left by one place. In this case, eqs. (3.1) and (3.2) become:

$$\Theta_{XY}(k) = \sum_{i=0}^{N-1} x_i x_{i+k} = \begin{cases} \dfrac{N+1}{2}, & k = 0 \\ \dfrac{N+1}{4}, & k = 1 \text{ to } N-1 \end{cases} \tag{3.5}$$

$$\text{and} \quad \Theta_{\bar{X}Y}(k) = \sum_{i=0}^{N-1} (1-x_i) x_{i+k} = \begin{cases} 0, & k = 0 \\ \dfrac{N+1}{4}, & k = 1 \text{ to } N-1 \end{cases} \tag{3.6}$$

The sum $i+k$ in eqs. (3.5) and (3.6) is taken modulo N. The previous results come from the shift-and-add property of m-sequences which says that the modulo-2 sum of an m-sequence and any cyclic phase shift of the same m-sequence is another phase of the same sequence [38].

By examining eqs. (3.5) and (3.6), we can see that the condition $\Theta_{XY}(k) = \Theta_{\bar{X}Y}(k)$ is satisfied. If we compute the difference between $\Theta_{XY}(k)$ and $\Theta_{\bar{X}Y}(k)$, we finally obtain:

$$Z = \Theta_{XY}(k) - \Theta_{\bar{X}Y}(k) = \begin{cases} \dfrac{N+1}{2}, & k = 0 \\ 0, & k = 1 \text{ to } N-1 \end{cases} \tag{3.7}$$

If we assign the N cycle shifts of a single unipolar m-sequence to the subscribers, complete orthogonality will be achieved. Therefore, such an optical CDMA system can support up to N simultaneous users without any interference.

3.1.2 Hadamard Codes

A Hadamard code is obtained by selecting as code words the rows of a Hadamard matrix [39]. A Hadamard matrix $\mathbf{M_N}$ is a $N \times N$ matrix of 1's and 0's with the property that any row differs from any other row in exactly $N/2$ positions. One row of the matrix contains all zeros. The others contain $N/2$ 0's and $N/2$ 1's. Excluding the row containing

all zeros, half of the matching elements between two rows are 1's and half are 0's. Hadamard codes are not periodic, therefore we will not consider their periodic crosscorrelation in the following development. If we select (**X**) as row i and (**Y**) as row j. the crosscorrelations of (**Y**) with (**X**) and with its complementary sequence are:

$$\Theta_{XY}(i,j) = \sum_{k=0}^{N-1} x_k\, y_k = \begin{cases} \dfrac{N}{2}, & \text{for } i = j \\ \dfrac{N}{4}, & \text{for } i \neq j \end{cases} \tag{3.8}$$

$$\text{and} \quad \Theta_{\overline{X}Y}(i,j) = \sum_{k=0}^{N-1} (1 - x_k) y_k = \begin{cases} 0, & \text{for } i = j \\ \dfrac{N}{4}, & \text{for } i \neq j \end{cases} \tag{3.9}$$

Once again, we see that the condition for user orthogonality is achieved (3.3) and the receiver equation in this case becomes:

$$Z = \Theta_{XY}(i,j) - \Theta_{\overline{X}Y}(i,j) = \begin{cases} \dfrac{N}{2}, & i = j \\ 0, & i \neq j \end{cases} \tag{3.10}$$

With the rows of a $N \times N$ Hadamard matrix, up to $N-1$ subscribers could be accommodated since the row with all zeros must be rejected.

In the next section, we will show the transmitter and receiver required to perform the encoding and decoding using one of the codes previously presented.

3.2 Transceivers Design

3.2.1 Encoding in the Frequency Domain

The main advantage of spectral CDMA encoding over time-domain CDMA encoding is that the bit rate is not multiplied by a spreading gain, since the coding is performed in frequency (or wavelength) and not in time. How is frequency encoding accomplished?

The addressing is performed by encoding the entire available linewidth at once with the sequence corresponding to the intended user. It is done directly onto the LED spectrum, which is not a function of the modulating signal. Therefore, the bit rate remains the same, regardless of the code length value. In the proposed scheme, the wavelength band is provided by a single noncoherent source, such as a LED or a SLD. The spectrum is spectrally sliced into equal power slots. The number of slots depends on the code length. After spectral slicing, each chip of the code sequence is assigned to a particular wavelength slot, as shown in Fig. 3.1. Wavelength slots corresponding to the 0's of the sequence are then filtered out from the LED spectrum, so that the code is reproduced on the spectrum.

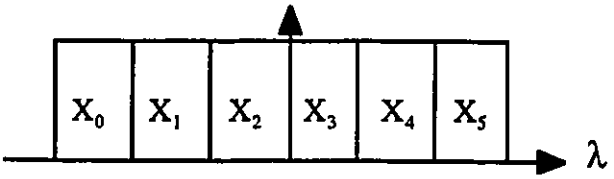

Fig. 3.1 Spectral slicing. The LED spectrum is sliced into N equal power slots and each slot is assigned with a chip x_i of a length N code sequence.

Filtering of wavelength slots can be done in different ways, like the use of acousto-optical tunable filters [24] or integrated planar optics such as arrayed waveguides and fiber Bragg gratings. State-of-the-art technologies are still very lossy today. Another approach is to spatially separate the different wavelengths of the spectrum and then block the undesired wavelengths slots with an amplitude mask, as shown in Fig. 3.2. This is the approach we concentrated on.

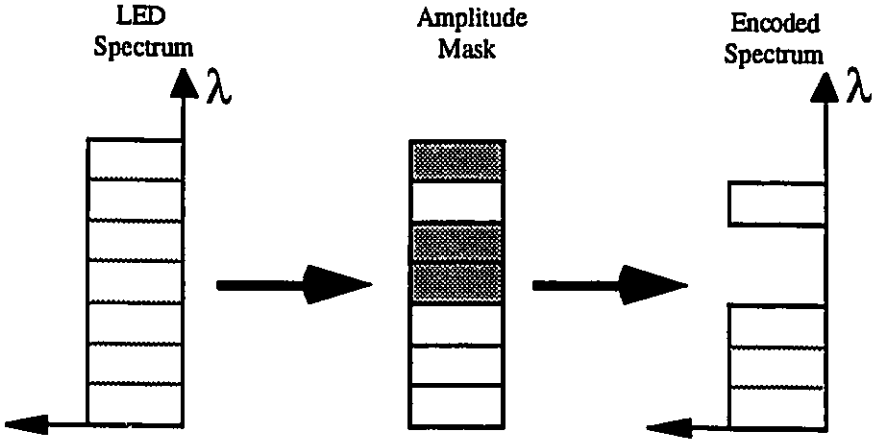

Fig. 3.2 LED spectrum filtering with an amplitude mask.

3.2.2 Coherent and Noncoherent Coding

Fig. 3.3 shows encoding of broad linewidth sources by a standard lens and grating apparatus. This set-up has been extensively used by Weiner, et al. for coherent phase encoding of ultrashort pulses [22]. In this method, a phase mask is used to scramble the spectral phases of the wavelength slots. Each pixel of the mask corresponds to a phase shift of zero or π. The pulse shape at the output of the second grating is the Fourier transform of the pattern transferred by the mask onto the frequency spectrum. To recover the pulse, the inverse Fourier transform has to be performed on the detected signal at the receiver, therefore exact Fourier and inverse Fourier transforms are necessary to encode and decode the data.

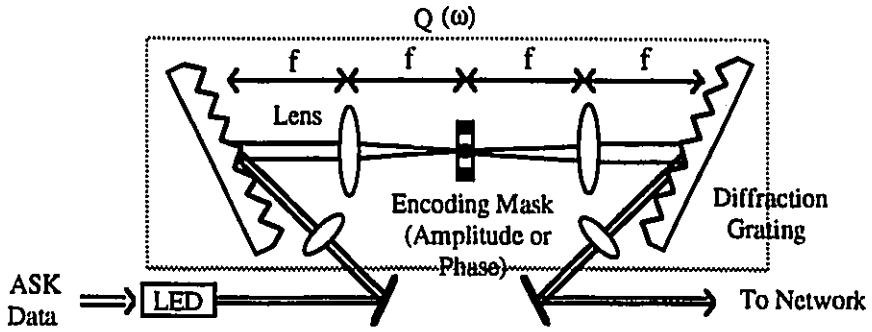

Fig. 3.3 Schematic Diagram of the encoding set-up. The optical signal is collimated on a grating, which angularly separates the different wavelengths. They are focused on a mask, recombined in a single beam by a second grating and sent to the network.

First, a binary data stream modulates the intensity of the source. The modulated optical signal is then sent to the frequency encoding apparatus, noted by $Q(\omega)$. It is collimated by a lens. The collimated light pulses $u(t)$ can be represented by :

$$u(t) = a(t)\exp(-i\omega_o t) \quad \text{with} \quad A(\omega) = \int_{-\infty}^{\infty} a(t)\exp(i\omega t)\,dt \tag{3.11}$$

where ω_o is the central frequency, $a(t)$ is the complex amplitude envelope with spectrum $A(\omega)$, and ω is the frequency shift from ω_o.

The collimated light beam illuminates a first grating placed in the front focal plane of a lens. The different wavelengths are angularly dispersed and focused on the back focal plane, where a spatially patterned mask is placed. In terms of Fourier optics, the effect of

the grating on the signal is the same as if plane waves pass through a transparency with the following complex amplitude transmission :

$$T(\omega,x)=t(x)\exp\left[ik\left(\frac{d\theta}{d\omega}\omega\right)x\right] \tag{3.12}$$

where x is the transverse coordinate in the front focal plane, $k=\frac{2\pi}{\lambda}$ is the wave propagation constant and $\frac{d\theta}{d\omega}$ is the angular dispersion of the grating derived from the grating equation and explained in Section 3.3.1. The expression in (3.12) is valid only for paraxial approximation. After the grating, the field distribution $V(\omega,x)$ becomes:

$$V(\omega,x)=t(x)A(\omega)\exp\left[ik\left(\frac{d\theta}{d\omega}\omega\right)x\right] \tag{3.13}$$

According to the Fourier transform properties of the lens, the field distribution $V_f(\omega,x_f)$ in the back focal plane is represented as:

$$V_f(\omega,x_f)=\exp\left\{i\frac{k}{2f}\left(1-\frac{d_o}{f}\right)x_f^2\right\}A(\omega)\int_{-\infty}^{\infty}t(x)\exp\left\{-\frac{2\pi i}{\lambda f}xx_f-\frac{2\pi i}{\lambda}\left(\frac{d\theta}{d\omega}\omega\right)x\right\}dx \tag{3.14}$$

where x_f is the coordinate space in the back focal plane, f is the lens focal length, and d_o is the distance between the grating and the lens, $d_o=f$ in this case. The first exponential in (3.14) is a phase factor associated with longitudinal and transverse misalignments. The encoding mask at the back focal plane with a complex transfer function $H(\xi)$ manipulates the frequency component structure of the field. After the mask, the amplitude distribution is proportional to:

$$\tilde{V}_f(\omega,\xi)\ \propto A(\omega)\tau\left(\xi-\left(\frac{d\theta}{d\omega}\frac{\omega}{\lambda}\right)\right)H(\xi) \tag{3.15}$$

where $\tau\left(\xi-\left(\frac{d\theta}{d\omega}\frac{\omega}{\lambda}\right)\right)$ is the Fourier transform in the spatial frequency domain (ξ) of the grating complex amplitude transmission, as given by (3.12). In the small angle approximation, the spatial frequency coordinate ξ is related to the spatial coordinate x by $\xi=\frac{x}{\lambda f}$. As seen from (3.15), the mask modulates the frequency structure of the passing

field by manipulation of its spatial structure. The coherent encoding can be performed on phase, amplitude or on both. After encoding, the second lens performs the inverse Fourier transform of the signal wave. The output field amplitude $V_o(\omega, x_i)$ is:

$$V_o(\omega, x_i) \propto \int A(\omega)\tau\left(\xi - \left(\frac{d\theta}{d\omega}\frac{\omega}{\lambda}\right)\right)H(\xi)\exp\{+2\pi i\xi x_i\}d\xi \qquad (3.16)$$

where x_i is the coordinate space in the back focal plane of the second lens. As seen, the transfer function of the mask is encoded into the spectral spatial structure of the output radiation. The light field illuminates a second grating where all the spectral components are recombined into a single optical beam which is sent back to the network. The inverse Fourier transform from frequency domain to time gives the temporal profile of the light pulse.

$$v(t, x_i) \propto \int A(\omega)\tau\left(\xi - \frac{d\theta}{d\omega}\frac{\omega}{\lambda}\right)H(\xi)\exp\{-2\pi i\xi x_i + i\omega t\}d\xi dt \qquad (3.17)$$

The code of the mask should match the one used by the intended receiver. The set-up of Fig. 3.3 is quite difficult to work with. As seen from the above equations (3.11) - (3.17), any longitudinal and transverse misalignment in this system will result in a multiplication by a spatial frequency phase factor explicated in (3.14) and will affect also the spectral structure of the signal wave. Therefore, exact Fourier transform is required to cancel all phase factors. This is why d_o is restricted to a value of f in (3.14). The presence of four different lenses makes the alignment procedure quite tedious, because precision is essential.

In the CDMA system invented by our research group [3-6], we perform incoherent encoding. In an incoherent system, the lens performs a linear transformation on the intensity. Therefore, in the Fourier plane we are interested in the intensity distribution of the light field (3.14).

$$I_f(\omega, x_f) = \left|V_f(\omega, x_f)\right|^2 = \left|\exp\left\{i\frac{k}{2f}\left(1 - \frac{d_o}{f}\right)x_f^2\right\}A(\omega)\right.$$
$$\left.\times\int_{-\infty}^{\infty} t(x)\exp\left\{-\frac{2\pi i}{\lambda f}xx_f - \frac{2\pi i}{\lambda}\left(\frac{d\theta}{d\omega}\omega\right)x\right\}dx\right|^2 \qquad (3.18)$$

As can be seen from the above equation, the phase factor will disappear, regardless of the value of d_o. Therefore, in terms of the Fourier transform, the grating is not necessarily placed in the front focal plane of the lens and misalignment will not affect the spectral structure of the processed field (as far as the phase factor is concerned). In the Fourier plane, we have now, the normalized spatial frequency intensity spectrum of the processed signal $\tilde{I}_{fm}(\omega,\xi)$ multiplied by the mask optical transfer function $G(\xi)$,

$$\tilde{I}_{fm}(\omega,\xi) \propto \tilde{I}_f(\omega,\xi)G(\xi) \tag{3.19}$$

where $G(\xi)$ for the noncoherent case and $H(\xi)$ for the coherent are related as [40]:

$$G(\xi) = \frac{\int H(\zeta)H^*(\zeta+\xi)d\zeta}{\int |H(\zeta)|^2 d\zeta} \tag{3.20}$$

3.2.3 Proposed Transmitter

As mentioned in the previous section, exact Fourier transform is not required for noncoherent CDMA, since the coding is performed on intensity and not on phase. The decoding principle relies on accumulated light intensity, therefore one does not care about phase recovery. The requirements imposed by spectral amplitude encoding on the optical set-up are different compared to a system based on phase encoding. Since there is no obligation to have exact optical Fourier, one single lens of shorter focal length can be used for both collimating and focusing.

Such an arrangement is known as Littrow mounting [41]. It is widely used in grating spectrographs. In traditional spectrographs, light from a narrow source in the focal plane of a lens is incident on a reflection grating, and the images of the sources formed by the diffracted rays are observed in the focal plane of a second lens. In a Littrow mounting, the first order diffracted beam returns along the path of the incident beam. The facet angle of the grooves (blaze angle) is such that the distribution of light among the diffracted orders is maximized for the first order. A grating in Littrow use is shown in Fig. 3.4.

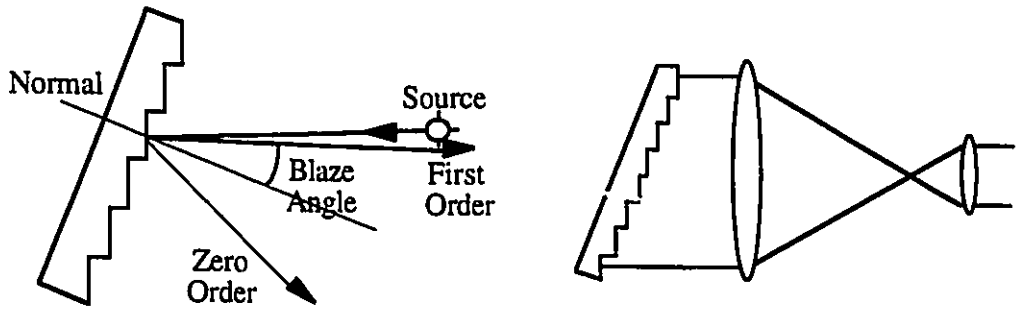

Fig. 3.4 Littrow mounting. (a) Grating in Littrow use. The diffracted beam returns along the path of the incident beam. (b) Littrow mounting. One lens serves the double purpose of collimating and focusing.

The arrangement in Fig. 3.4 (b) exploits the property of gratings in Littrow use. Since the first order diffracted beam and the incident beam are almost parallel, one lens can collimate the incident rays and focus the diffracted ones. Therefore, the source and the spectrum will both lie in the same plane. If we place a spatially patterned mask at the focal plane of the lens, Littrow mounting can be used as an optical CDMA encoder. This arrangement has the advantage of compactness. This allows a reduction of the number of optical components in the transmitter, so to decrease losses. The proposed system is shown in Fig. 3.5.

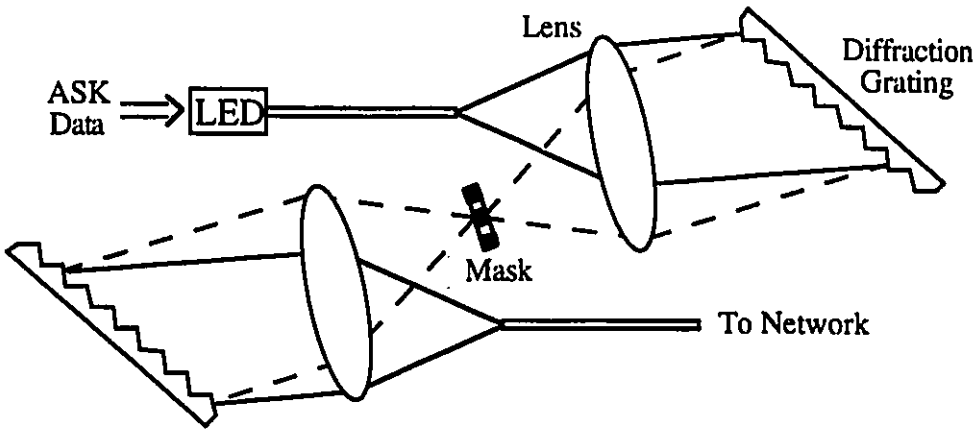

Fig. 3.5 Proposed transmitter. One lens is used for both beam collimation and focusing

The modulated LED light is first coupled into a multi-mode fiber. At the output end of the fiber, the signal expands and is collimated by a lens before falling onto a reflection

grating. Different wavelengths are separated and focused by the same lens onto different spots on an amplitude code mask. After spectrum encoding, the beam passes through a second lens-grating apparatus. All spectral components emerge from it at the same angle and are focused into an optical fiber.

This set-up can be simplified even more if the grating is slightly tilted with respect to the plane of the page, and a reflective mask is used instead of a transmissive mask. From Fig. 3.4 (b), it can be seen that the collimated light after encoding will be focused on a point close to the source, where it can be coupled back into an optical fiber. The bars of the mask corresponding to 1's would be reflective, as the bars corresponding to 0's would absorb the light falling onto them. If such a mask is put in the set-up, then a single lens-grating apparatus can be used to angularly separate the wavelengths before encoding and recombining them after falling onto the mask. Such a set-up would only require one lens and one grating, as seen in Fig. 3.6.

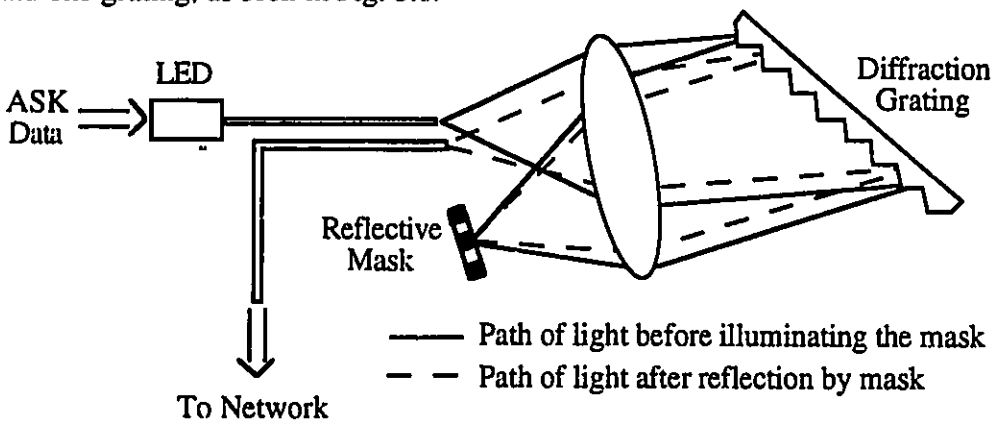

Fig. 3.6 Modification to the proposed transmitter. The mask is reflective, therefore the same lens and grating apparatus is used for wavelength separation and recombining.

3.2.4 Decoding Procedure

The receiver needs to compute eq. (3.4). It has been suggested by Zaccarin and Kavehrad [3,4] to use a differential receiver using 2 photodetectors, one to receive $\Sigma x_i x_{i+k}$, the other to receive $\Sigma(1-x_i)x_{i+k}$, and then subtracting their output. The required receiver is shown in Fig. 3.7.

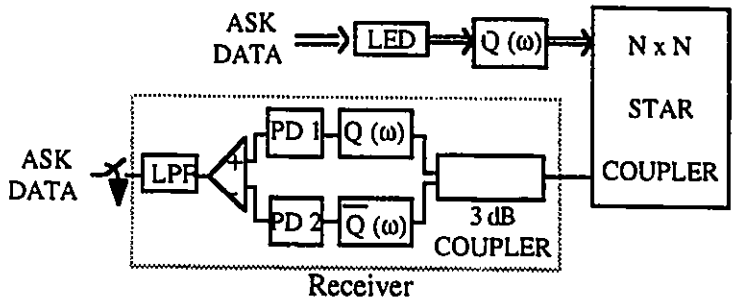

Fig. 3.7 Schematic diagram of the receiver. The signal is split into two parts, each one redirected to a lens-grating apparatus. The mask pattern in one arm is the complementary of the one used in the other arm.

In Fig. 3.7, the block $Q(\omega)$ denotes the lens-grating apparatus with the encoding mask as depicted in Fig. 3.3. The network consists of a simple $N \times N$ star coupler, N being the number of users in the network. A differential receiver (noted by the block in Fig. 3.7) is placed at each output of the star coupler. To develop the detection rule, it is required to split the incoming light signal into two parts, each passing through a different branch. On each branch, a lens-grating apparatus and a mask are required, as in Fig. 3.3. The mask pattern in one branch needs to be the complementary of the one used in the other branch. This opposite branch is noted $\overline{Q}(\omega)$ in Fig. 3.7.

The electrical current generated by a photodetector is directly proportional to the number of photons it detects (optical power detected). Theoretically, the average number of photons in all the wavelength slots is the same (Fig. 3.2), so the optical power in each slot is the same. If the code words used in the transceivers are such that $\Theta_{XY}(k) = \Theta_{\overline{X}Y}(k)$ for $k \neq 0$, then in the case of an unfriendly user, the power detected in each arm will be equal. When subtracting the electric currents generated by each photodetector, they will cancel out each other since they will be equal. Let's illustrate the detection procedure with an example.

In Section 3.1, we computed the necessary crosscorrelations for an m-sequence code, which are :

$$\Theta_{XY}(k) = \begin{cases} \dfrac{N+1}{2}, & k = 0 \\ \dfrac{N+1}{4}, & k = 1 \text{ to } N-1 \end{cases} \quad \text{and} \quad \Theta_{\overline{X}Y}(k) = \begin{cases} 0, & k = 0 \\ \dfrac{N+1}{4}, & k = 1 \text{ to } N-1. \end{cases}$$

$$\Theta_{XY}(k) = \begin{cases} \dfrac{N+1}{2}, & k = 0 \\ \dfrac{N+1}{4}, & k = 1 \text{ to } N-1 \end{cases} \quad \text{and} \quad \Theta_{\overline{X}Y}(k) = \begin{cases} 0\ , & k = 0 \\ \dfrac{N+1}{4}, & k = 1 \text{ to } N-1. \end{cases}$$

In Fig. 3.7, the receiver branch noted by $Q(\omega)$ computes $\Theta_{XY}(k)$. For an unfriendly user ($k \neq 0$), the power detected by the photodetector will be equal to $(\frac{N+1}{4})P_S$, where P_S is the optical power in a wavelength slot. The power detected in $\overline{Q}(\omega)$ will also be equal to $(\frac{N+1}{4})P_S$. The electric current produced by the two photodetectors will be the same, since proportional to the same detected power. Subtracting these two equal currents will lead to a resulting mean current of 0. For a friendly user ($k = 0$), the current produced by the photodetector in $Q(\omega)$ will be proportional to $(\frac{N+1}{2})P_S$, while it should be null in $\overline{Q}(\omega)$, since the detected power is 0. So a subtraction of the currents will give a non-zero output current. The signal is detected by the intended user. The procedure is illustrated in Fig. 3.8.

If a user decides to communicate with user j in a network, the mask at its transmitter should match the sequence of user j. Each time a non-zero bit is sent, the LED is turned on for on-off keying modulation and its spectrum is encoded with the destination address, e.g. the address of user j. The signal is sent to all the users in the network through a $N \times N$ star-coupler. User i receives the signal. It is first split in two and redirected to the two branches of the differential receiver. On the amplitude mask noted "MASK" is reproduced the address of user j, while "$\overline{\text{MASK}}$" denotes the complementary mask. In both arms, only one wavelength slot passes through the amplitude mask. Therefore, the two photodetectors will detect the same optical power, they will produce electrical currents of equal intensity, and their subtraction will lead to a zero-current. The signal will remain undetected by user i.

At the receiver of user j, the mask noted "MASK" doesn't block any wavelength slot since the code on the mask and on the received signal are the same. As for the complementary mask, it filters out the entire received signal since the codes are complementary (the crosscorrelation between a binary code and its complement is 0). Consequently, the photodetector in the complementary branch produces no electric current,

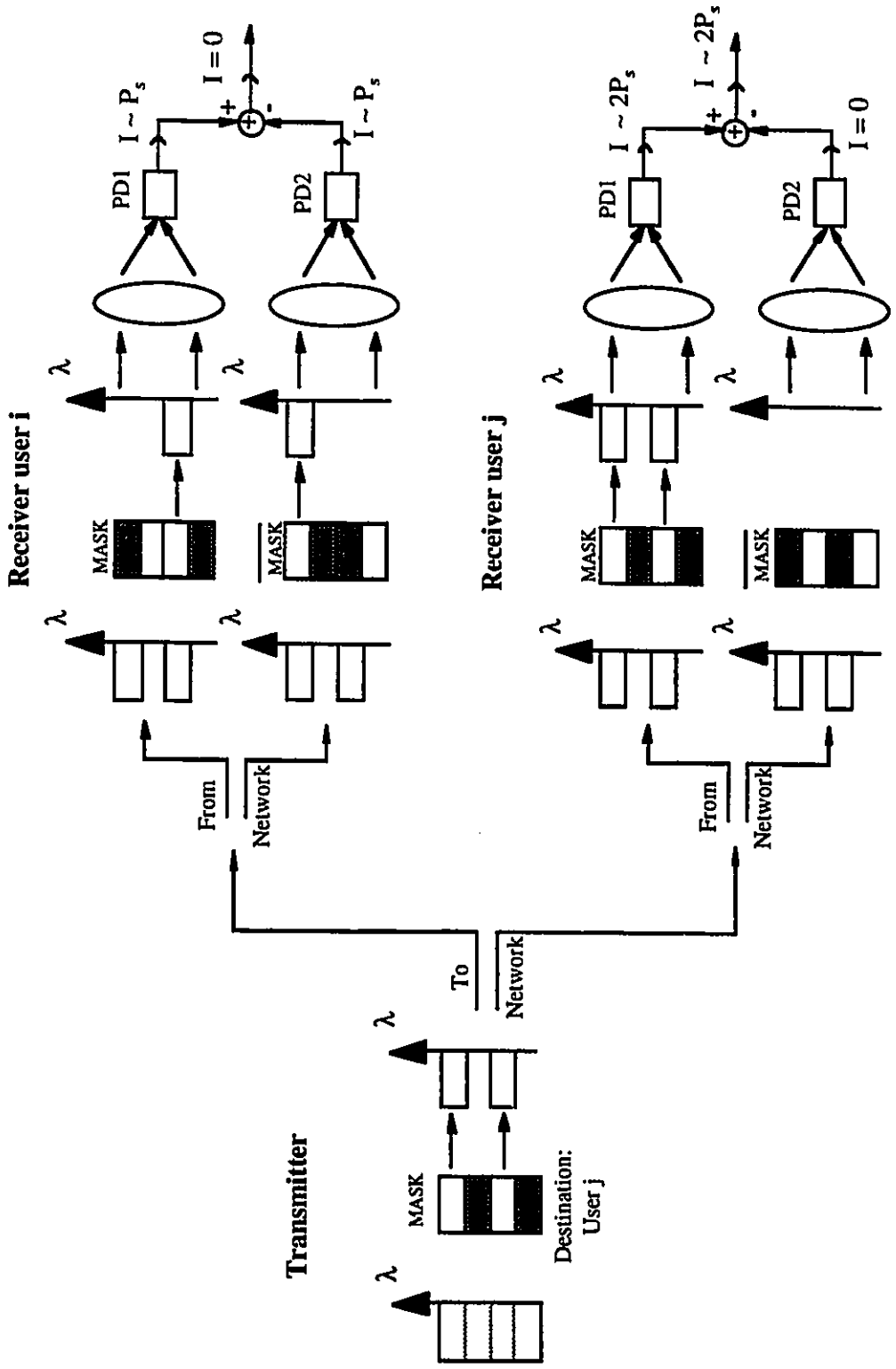

Fig. 3.8 Decoding principle. For an unfriendly user, the detector receives the same power in each arm. For a friendly user, the detector associated with the complementary mask receives no optical power.

3.2.5 Proposed Receiver

As previously mentioned, Zaccarin and Kavehrad [3,4] have proposed a differential receiver with two photodetectors in order to compute eq. (3.3), illustrated in Fig. 3.7. They have suggested to split the incoming signal into two parts, each part going through a separate lens and grating apparatus. This approach leads to a very complicated set-up, requiring four different gratings [24].

Indeed, one has to make sure that the spectrum focused on the masks is exactly the same in both arms, else a loss of orthogonality could be observed. The presence of many lenses and gratings makes this job very tedious, if not impossible. It would be preferable to use the same lens and grating apparatus for both arms. Fig. 3.9 illustrates the proposed receiver.

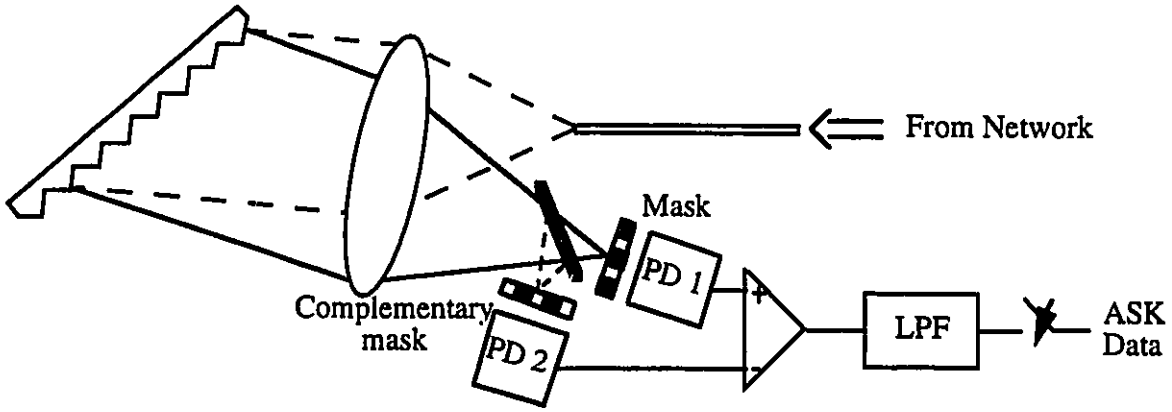

Fig. 3.9 Proposed receiver.

The optical signal exits the optical fiber and passes through the lens and the grating. A beamsplitter splits the diffracted beam. One beam is focused onto an amplitude mask corresponding to the address of this particular user, while the second beam is focused onto the complementary mask. The unfiltered wavelengths are directly focused onto the receiving area of the two photodetectors.

In this receiver, the signal is split just before entering the masks. Therefore, the light follows the same optical path and the spectrum is the same in both arms. With such a set-up, the number of optical components in the receiver is reduced to a minimum, greatly increasing compactness and decreasing optical losses.

As specified in [3], the second grating used to recombine the unfiltered wavelengths at the transmitter is not needed in the receiver since the spectral components can be directly focused onto the photodetector, consequently simplifying the receiver. We have reduced the originally proposed receiver set-up from four gratings to only one. Besides, it would be impossible to obtain an image spot after the second grating, small enough to focus all the optical power back into an optical fiber because of off-axis operation (see Section 3.3.3). Also, each wavelength follows a different optical path in the system, making it impossible to focus all the wavelengths into a single spot. Therefore, by placing a second grating, we would unnecessarily lose optical power.

3.2.6 Receiver Electronics

In Fig. 3.10 is depicted the required electronic amplification and processing circuits for the system. First, each photodetector detects the light and the signals are amplified before subtraction. The resulting signal is amplified and compared to a threshold level. After a decision is made, the signal is fed through a TTL level driver, in order to match the impedance of the digital transmission analyzer. Each block in Fig. 3.10 is detailed in the Appendix.

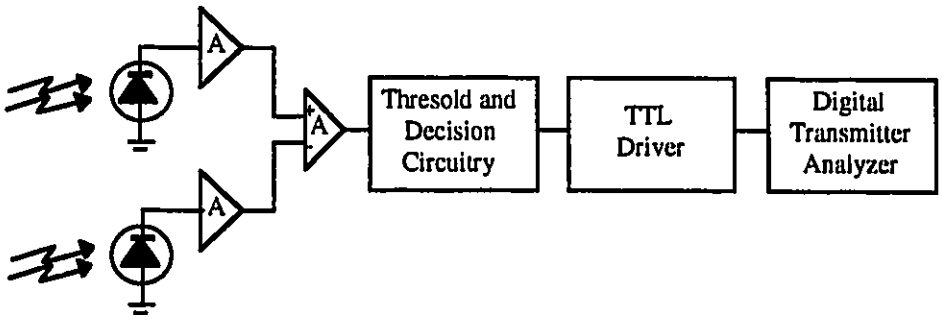

Fig. 3.10 Electronic circuit for signal recovery.

3.3 Optical Parameters of Transceivers and Their Impact on System Capacity

Multi-user capacity is an extremely important factor to consider in any network. We refer to this capacity as the maximum number of users supported by a network without any inter-user interference. Theoretically, such a capacity for an amplitude encoded CDMA system strictly depends on the length of the encoding/decoding sequences. In practice however, any spectral apparatus has a limited resolution, that is the smallest wavelength separation it can resolve. As a result, the LED spectrum cannot be sliced indefinitely and the wavelengths slots in Fig. 3.1 must have a minimum width. This will therefore limit the code length that can be accommodated by the spectral apparatus. In this section, we will explain how the optical parameters of the proposed transceivers (e.g., focal length of lenses, grating pitch, numerical aperture of input fiber) affect the system capacity, and relate these parameters to the experiment. The interested reader may refer to [42,43] for a complete description.

3.3.1 Diffraction-Limited Performance

In a diffraction-limited spectral apparatus, the resolving power $\lambda/\Delta\lambda$ is a measure of the ability to separate neighboring spectral lines of slightly different wavelengths. In an image-forming system (non diffraction-limited), it is a measure of the ability to separate images of two object points and is expressed as $1/\delta x$ or $1/\Delta\theta$, where δx and $\Delta\theta$ are respectively the minimum distance or minimum angle between the two images. In the absence of aberrations, a point object gives rise to a sharp point image. Because of diffraction, however, the actual image is a spot of a finite size, i.e., a diffraction pattern. The two-dimensional Fraunhofer diffraction pattern by a circular aperture of radius a is given by the well-known expression [42]:

$$I = I_0\left[\frac{2J_1(\rho)}{\rho}\right]^2 \tag{3.21}$$

where $I = I(\rho)$ is the intensity at coordinate $\rho = ka\sin\theta$, k the propagation constant, θ the angle of the beam, I_0 the intensity at $\theta = 0$, and $J_1(\rho)$ is the Bessel function of the first order (Fig. 3.11 (a)). The diffraction pattern is plotted in Fig. 3.11 (b), and the alternating light and dark circles corresponding to this intensity pattern are also shown. The bright central area is known as the Airy disc. The first dark ring corresponds to the first zero of the Bessel function for which $\rho = 3.832$. Since $\sin\theta = \frac{\rho}{ka}$, we have approximately :

$$\theta = \frac{3.83\lambda}{2\pi a} = \frac{1.22\lambda}{D} \tag{3.22}$$

where $D = 2a$ is the diameter of the diffracting circular aperture. In the proposed transceivers, the entrance pupil of the system acts as the diffracting aperture. The entrance pupil of the system is determined by the numerical aperture of the fiber and the lens focal length, as seen on Fig. 3.12.

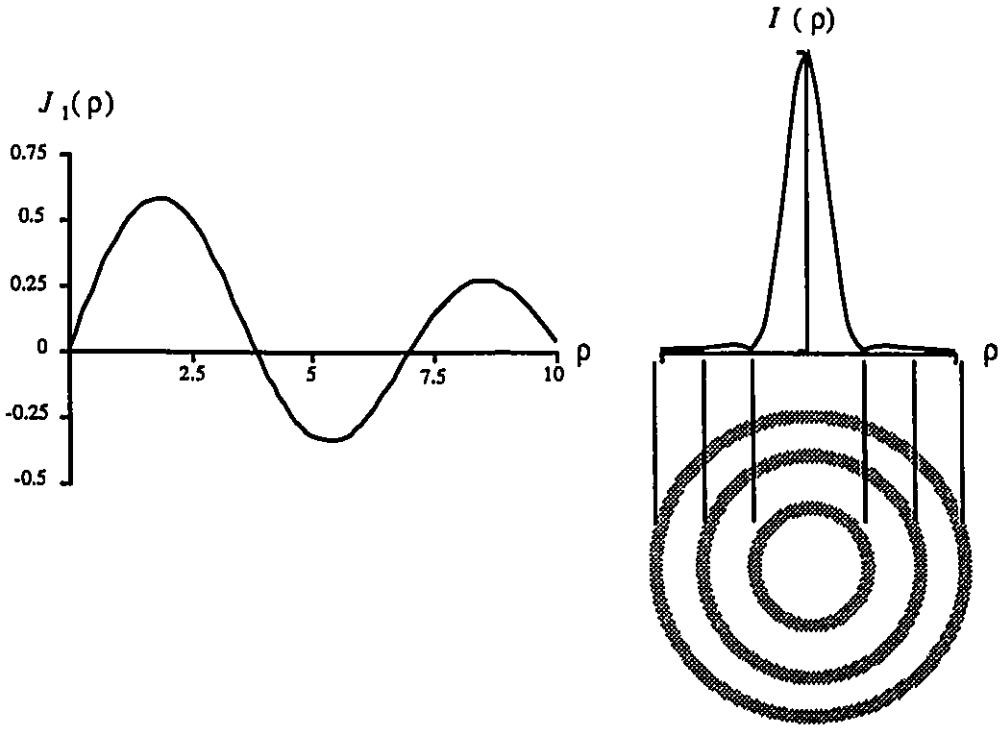

Fig. 3.11 (a) Bessel function of the first kind. (b) Two-dimensional Fraunhofer diffraction pattern by a circular aperture. The alternating light and dark circles correspond to the intensity pattern.

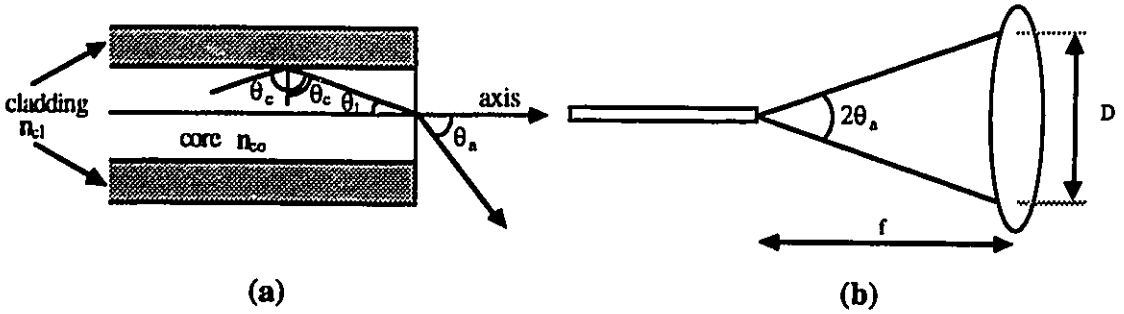

Fig. 3.12 (a) Numerical aperture of fiber. (b) Entrance pupil of system.

As a reminder, the numerical aperture of an optical fiber is defined as $NA = \sin\theta_a$, where θ_a is the acceptance angle which is the maximum entrance angle for an optical ray to be guided by the fiber by total internal reflection (TIR). In Fig. 3.12 (b), D is the diameter of the entrance pupil (diffracting aperture) and f is the focal length of the lens. It is easy to find that :

$$NA = \sin(\theta_a) = \frac{D/2}{f} \quad \Rightarrow \quad D = 2f(NA) \tag{3.23}$$

Expression (3.22) also gives the minimum angular separation of two points whose Airy discs might be distinguished in the image plane. If the angular spacing is $1.22\lambda/D$, then the central maximum of one disc corresponds to the first zero of the other one. It is called Rayleigh's criterion, and is shown in Fig 3.13 (a).

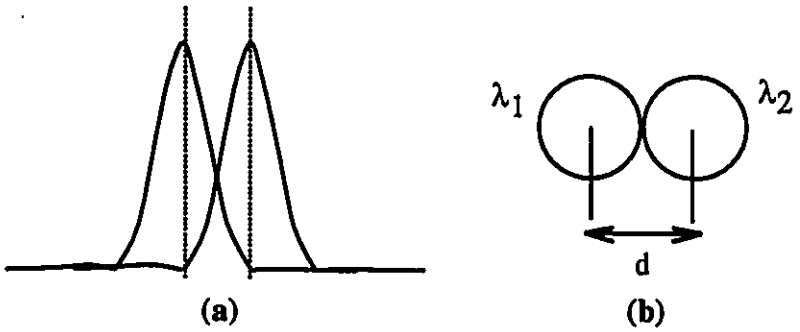

Fig. 3.13 Spectral resolution. (a) Rayleigh's criterion. Two adjacent Airy disks might be distinguished if the central maximum of one disc corresponds to the first zero of the other one. (b) For the non diffraction-limited case, two wavelengths are resolved if their monochromatic images of the source can be resolved.

Expression (3.22) tells us that the resolution of a system, neglecting aberrations, is improved by increasing the entrance pupil diameter. It can be done in two ways: using a lens with longer focal length or fiber with larger NA. The parameters δx and $\Delta\theta$ are related by the expression $\Delta\theta/2 = \tan(\Delta\theta/2) = \delta x/(2f)$. Therefore, for a perfect collimation at unit magnification, the diffraction-limited resolution and the resolving of the lens system for a circular aperture and incoherent illumination are given as :

$$\delta x = 0.61\frac{\lambda}{NA} \cong 1.4\ [\mu m]; \quad \frac{1}{\delta x} \cong 7x10^2\ \left[mm^{-1}\right]; \tag{3.24}$$

where $\lambda = 830$ nm is the nominal wavelength entering the optical system and $NA = 0.37$ is the numerical aperture of the multi-mode fiber used in the experiment.

The grating dispersion is described by the grating equation [40], i.e.,

$$\sin\alpha_{inc} - \sin\alpha_{diff} = \frac{\lambda}{\Lambda} \tag{3.25}$$

where α_{inc} and α_{diff} are the corresponding angles of the incident and diffracted beams, Λ is the grating period. For the ideal Littrow grating configuration, the first-order diffracted beam comes back in the incident direction. The approximation $\alpha_{inc} = \alpha_{diff}$ provides useful information, although it is not exactly the case in the proposed transceivers. In a typical spectrograph arrangement, the incident angle α_{inc} is fixed, only the diffraction angle varies accordingly to the wavelength. We can rewrite the wavelength dependence of α_{diff} by $\alpha_{diff} = \alpha_{inc} + \delta$, where $\delta = \delta(\lambda)$. By differentiating the grating equation (3.25), we obtain the expression for the angular grating dispersion:

$$\frac{d\delta}{d\lambda} = \frac{1}{\cos(\alpha_{inc} + \delta)\Lambda} = \frac{2\tan(\alpha_{inc} + \delta)}{\lambda} \approx 1.3x10^{-3}\ \left[\text{nm}^{-1}\right] \tag{3.26}$$

The angular dispersion in (3.26) is related to the angular dispersion in eq. (3.12) by:

$$\frac{d\delta}{d\lambda} = \frac{\omega^2}{2\pi c}\frac{d\delta}{d\omega}.$$

The linear dispersion depends on the focal distance of the lens used. For a focal plane perpendicular to the diffracted beam, the linear dispersion is

Expression (3.22) tells us that the resolution of a system, neglecting aberrations, is improved by increasing the entrance pupil diameter. It can be done in two ways: using a lens with longer focal length or fiber with larger NA. The parameters δx and $\Delta\theta$ are related by the expression $\Delta\theta/2 \approx \tan(\Delta\theta/2) \approx \delta x/(2f)$. Therefore, for a perfect collimation at unit magnification, the diffraction-limited resolution and the resolving of the lens system for a circular aperture and incoherent illumination are given as :

$$\delta x = 0.61\frac{\lambda}{NA} \cong 1.4\ [\mu m]; \quad \frac{1}{\delta x} \cong 7x10^2\ \left[mm^{-1}\right]; \tag{3.24}$$

where $\lambda = 830$ nm is the nominal wavelength entering the optical system and $NA = 0.37$ is the numerical aperture of the multi-mode fiber used in the experiment.

The grating dispersion is described by the grating equation [40], i.e.,

$$\sin\alpha_{inc} - \sin\alpha_{diff} = \frac{\lambda}{\Lambda} \tag{3.25}$$

where α_{inc} and α_{diff} are the corresponding angles of the incident and diffracted beams, Λ is the grating period. For the ideal Littrow grating configuration, the first-order diffracted beam comes back in the incident direction. The approximation $\alpha_{inc} = \alpha_{diff}$ provides useful information, although it is not exactly the case in the proposed transceivers. In a typical spectrograph arrangement, the incident angle α_{inc} is fixed, only the diffraction angle varies accordingly to the wavelength. We can rewrite the wavelength dependence of α_{diff} by $\alpha_{diff} = \alpha_{inc} + \delta$, where $\delta = \delta(\lambda)$. By differentiating the grating equation (3.25), we obtain the expression for the angular grating dispersion:

$$\frac{d\delta}{d\lambda} = \frac{1}{\cos(\alpha_{inc} + \delta)\Lambda} = \frac{2\tan(\alpha_{inc} + \delta)}{\lambda} \approx 1.3x10^{-3}\ \left[\text{nm}^{-1}\right] \tag{3.26}$$

The angular dispersion in (3.26) is related to the angular dispersion in eq. (3.12) by:

$$\frac{d\delta}{d\lambda} = \frac{\omega^2}{2\pi c}\frac{d\delta}{d\omega}.$$

The linear dispersion depends on the focal distance of the lens used. For a focal plane perpendicular to the diffracted beam, the linear dispersion is

resolved, as illustrated in Fig. 3.13 (b). Neglecting diffraction, we can still use Rayleigh's criterion to find the linear resolution. Setting $\delta x = d = d'$ in (3.28), we find the spectral resolution of the optical system :

$$\delta\lambda = \frac{d}{f\dfrac{d\delta}{d\lambda}} \equiv 2 \text{ [nm]} \tag{3.29}$$

The minimum wavelength slot width must theoretically be 2 nm for it to be resolved. The system is therefore able to accommodate an optical code of (62/2)=31 chips with a 3 dB bandwidth of 62 nm coupled into the optical fiber. It is extremely small compared to the diffraction-limited case, where a possible number of 3100 users was evaluated. So one must find an acceptable trade-off between the low coupled power into single-mode fibers and the reduced number of possible subscribers when using multi-mode fibers.

The main limitation of optical CDMA comes from the severe losses experimented with the encoding and from the need to broadcast the signal to all the users without any optical amplification. A finer system resolution physically translates in a larger spatial spread of the spectrum, but also in less and less power per unit of area. After encoding, the extinction ratio, that is the ratio of power in a 1 to the power in a 0, will decrease and this can lead to a loss of orthogonality among adjacent users. In the next paragraphs, some ways to increase the power per unit of area without sacrificing the resolution are presented.

The radiant intensity is defined as the power per unit solid angle. The radiant intensity entering the transmitter is given by [42] :

$$J\left[\frac{\text{W}}{\text{sr}}\right] = \pi r^2 \frac{\pi a^2}{f^2} R; \quad R\left[\frac{\text{W}}{\text{cm}^2\text{sr}}\right] \tag{3.30}$$

where R is the radiance (intensity per unit of source area), $r = d/2$ is the radius of the fiber core (source), $a = D/2$ the radius of the entrance pupil, and f is the focal length of the lens. Accounting for the reflection losses (6% at each passage through the lens) and the

resolved, as illustrated in Fig. 3.13 (b). Neglecting diffraction, we can still use Rayleigh's criterion to find the linear resolution. Setting $\delta x = d = d'$ in (3.28), we find the spectral resolution of the optical system :

$$\delta\lambda = \frac{d}{f\dfrac{d\delta}{d\lambda}} \equiv 2 \text{ [nm]} \tag{3.29}$$

The minimum wavelength slot width must theoretically be 2 nm for it to be resolved. The system is therefore able to accommodate an optical code of (62/2)=31 chips with a 3 dB bandwidth of 62 nm coupled into the optical fiber. It is extremely small compared to the diffraction-limited case, where a possible number of 3100 users was evaluated. So one must find an acceptable trade-off between the low coupled power into single-mode fibers and the reduced number of possible subscribers when using multi-mode fibers.

The main limitation of optical CDMA comes from the severe losses experimented with the encoding and from the need to broadcast the signal to all the users without any optical amplification. A finer system resolution physically translates in a larger spatial spread of the spectrum, but also in less and less power per unit of area. After encoding, the extinction ratio, that is the ratio of power in a 1 to the power in a 0, will decrease and this can lead to a loss of orthogonality among adjacent users. In the next paragraphs, some ways to increase the power per unit of area without sacrificing the resolution are presented.

The radiant intensity is defined as the power per unit solid angle. The radiant intensity entering the transmitter is given by [42] :

$$J\left[\frac{\text{W}}{\text{sr}}\right] = \pi r^2 \frac{\pi a^2}{f^2} R; \quad R\left[\frac{\text{W}}{\text{cm}^2\text{sr}}\right] \tag{3.30}$$

where R is the radiance (intensity per unit of source area), $r = d/2$ is the radius of the fiber core (source), $a = D/2$ the radius of the entrance pupil, and f is the focal length of the lens. Accounting for the reflection losses (6% at each passage through the lens) and the

diffraction efficiency of the grating ($\eta = 65\%$ at 830 nm), the intensity is reduced by a factor $T = T_{lens}^2 \eta = 0.6$. The radiant intensity J at the focal plane where the spectral coding takes place becomes :

$$J = T\frac{\pi r}{2}\frac{\pi a^2}{f}\left(\frac{d\delta}{d\lambda}\right)\delta\lambda N \tag{3.31}$$

The irradiance H[W/cm^2] [43] is found by multiplying J by the solid angle $\pi r^2/f$:

$$H = T\frac{\pi a^2}{2rf}\left(\frac{d\delta}{d\lambda}\right)\delta\lambda N = T\pi N\frac{a^2}{f^2} = TN\frac{\pi a^2}{r^2}\left(\frac{2\tan(\alpha_{diff})}{\lambda}\right)^2\delta\lambda^2 \tag{3.32}$$

As CDMA is power-limited, it is important to try to increase the power without sacrificing the resolution. In (3.32), one can see that the irradiance depends on the spectral resolution $\delta\lambda$. Increasing $\delta\lambda$ will also increase the irradiance, but will translate in less and less users being accommodated by the system. From (3.32), it is possible to modify the geometry of the system in order to increase the power. A large entrance pupil (a) and a short focal length (f) increase the irradiance at the spectral plane, as seen from (3.32). But from (3.29), the spectral resolution is inversely proportional to the focal length. A shorter focal length implies an increase in the minimum wavelength separation. Reducing the image size (r) of the source also increases the irradiance, but implies using fibers with smaller cores which reduce the coupling efficiency. A larger diffraction angle also improves the intensity in the spectral image as well as the spectral resolution of the system. However, the lens aberrations impose deterioration of image quality and resolution. Other factors that affect the spectral intensity and resolution are the SNR ratio, stray light from the mask and overlapping of the spectral components due to misalignment, imperfect collimation and aberrations. The idea is to find a compromise between compactness, optical spectral resolution and power.

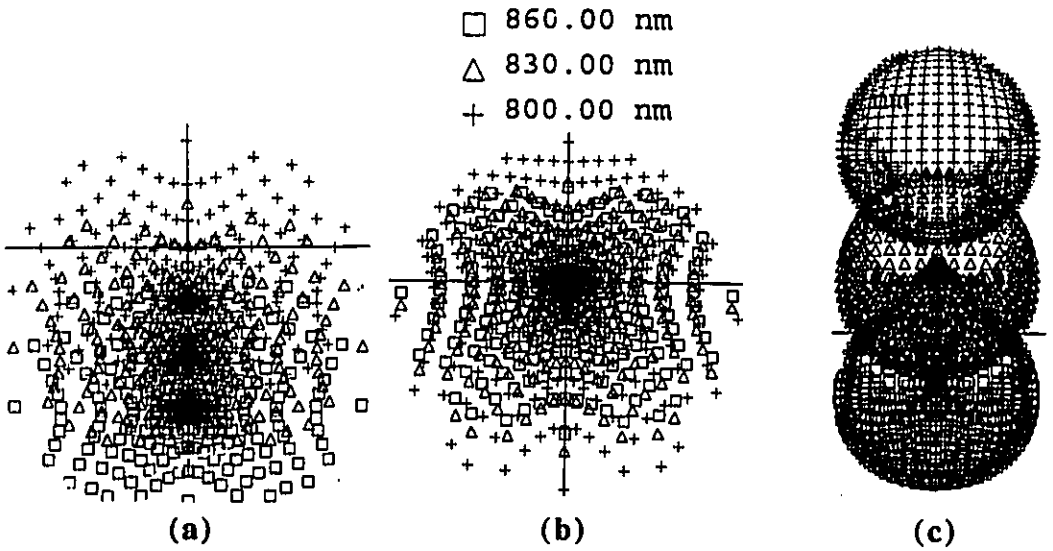

Fig. 3.14 Spot diagrams (a) at the spectral plane of the amplitude encoding, (b) at the plane where the light is coupled to the optical fiber, and (c) in the plane of the photodetectors aperture.

Off-axis operation also limits the amount of encoded light that can be broadcasted to the network. In Fig. 3.14 (b), the total power is focused over a large spatial region. According to the ray tracing, about 25% of the energy is focused on a spot size of diameter 200 μm at the focal plane of the second lens which corresponds to the core diameter of the multi-mode fiber used for the experiment. This means that at most 25% of the total power can be coupled in the fiber, neglecting reflection losses at the fiber surface. The distribution of accumulated power as a function of spot size radius is shown in Fig. 3.15.

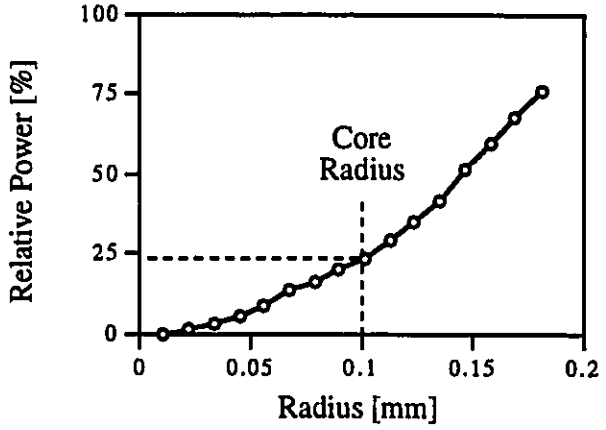

Fig. 3.15 Cumulative Radial Power distribution at the output focal plane of the transmitter. Approximately 25% of the light is concentrated on a 200 μm diameter spot size, corresponding to the multi-mode fiber core diameter.

In Fig. 3.14 (c) is shown the spot diagram at the photodetectors aperture plane in the receiver. According to the ray tracing, the small collecting lenses used fill the detectors apertures. The spot diagram has a transversal width of approximately 10 mm which is less than the photodetector aperture diameter of 11.3 mm. As previously mentioned, the second grating used to recombine the wavelength is not necessary. That is why a spatial separation of the spectral components is still observed at the photodetector plane. The spectral response of the photodetector over the wavelength range of 800 to 860 nm is a constant. In fact, photodetectors generally have an extremely large bandwidth. Therefore, it does not matter if one particular wavelength is concentrated onto a particular area of the photodetector, as long as the total illumination is equally distributed over the photodetector aperture.

Figs. 3.16 (a) and (b) show the geometrical ray tracing plots for the transmitter and receiver, respectively. The intersection of many rays in the vicinity of the focal plane indicates that a monochromatic image of the source is formed at that point. It one would place a screen perpendicular to the page at the focal plane of the transmitter and at the photodetector plane, he would observe the spot diagrams in Fig. 3.14 (a) and (c). As it can be seen, no clear monochromatic image is achievable. Furthermore, the monochromatic images of the three wavelengths are not located in the focal plane, not even in the same plane.

The reason for this situation is the use of a large aperture spherical lens [42]. For light rays traveling close to the optical axis also known as paraxial rays, the image will be located in the focal plane. The marginal rays propagating far from the optical axis will see different focal lengths, according to their longitudinal and transversal directions. These rays will tend to be focused closer to the lens, compared to the paraxial rays. In the experiment, the source was located a few millimeters away from the optical axis, in order to place the mask and the output fiber in the same plane and the source tilt was not negligible. Therefore

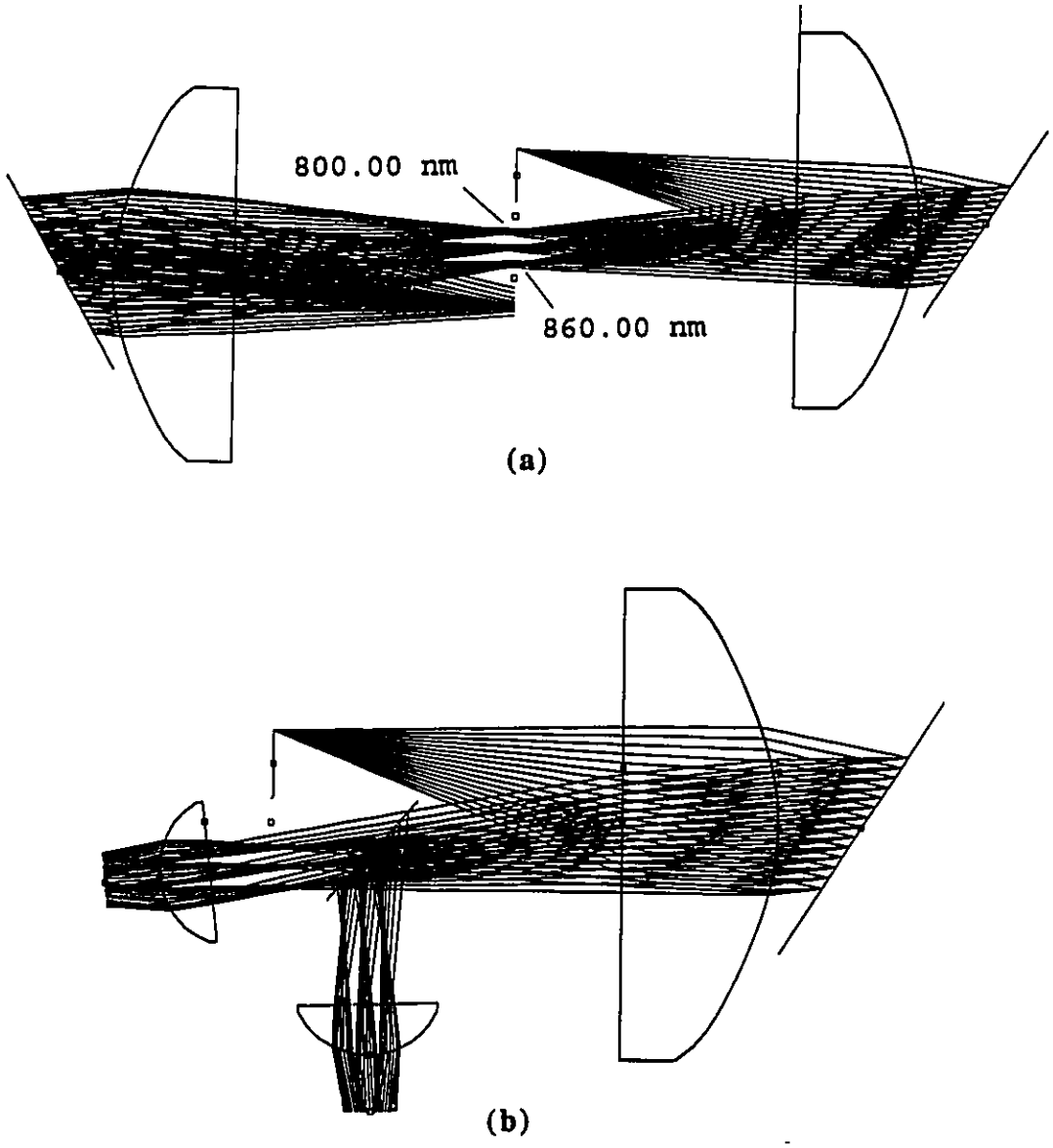

Fig. 3.16 Geometrical ray tracing plots for (a) the transmitter and (b) the receiver. The ray tracing was carried out for the nominal wavelength 830 nm and at the short and long ends of the 3 dB bandwidth, respectively 800 nm and 860 nm. Also shown, are the focal planes where the masks should be placed.

the longest wavelengths were focused closer to the lens compared to the shorter wavelengths traveling closer to the optical axis. This is why the mask was not located exactly in the focal plane, so as to achieve the best possible extinction ratio. The problems

of geometrical aberrations are inherent to situations where the paraxial approximation is not valid, that is, when using the full aperture of a lens. However, the spherical lens used in the experiment was of shorter focal length than an ordinary spherical lens with identical aberrations.

3.4 Practical Considerations for System Implementation

In this section, we consider two problems that can arise when implementing this system as a network or a switch. We first mention the requirements for the amplitude mask. We finally consider a few alternatives to the problem of the shape of the LED spectrum.

3.4.1 Amplitude Masks

Incoming data bits need to be routed to all the users in the network. The mask used in the transmitter can be made programmable so that its code can match the one of the intended receiver. Programmable masks can be achieved by using liquid crystal devices. The speed at which the reprogramming can be performed is of concern for switching. At present, spatial light modulators (SLM) with programming time in the nanosecond range exist but their contrast ratio is very low [44]. Devices with good contrast ratio and programming time in the milliseconds have been reported [45].

3.4.2 Spectral shape of the LED

In Section 3.1, it was assumed that all the 1's in the sequence would appear as 1's at the photodetector. However, the spectrum of a LED is not flat, but might exhibit for example a Gaussian shape. Consequently, the 1's will be seen at different values depending on the position they take along the spectrum. Therefore, the codes will appear as

being multilevel, and the perfect orthogonality between users will be lost. To counter this effect, the simplest solution is to reduce the length of the total encoded spectral band, to concentrate on the portion of the spectrum that is relatively flat, for example the 3 dB bandwidth of the LED. One can also use specially fabricated masks, having different lengths depending on the chips positions in the codes, so that the power transmitted in each band would be the same. Another solution is to equalize the LED spectrum with acousto-optic tunable filters. in the same ways they have been used in optical systems with amplifiers [46].

Chapter 4

An Experiment on the Proposed System

In this chapter, we present results of a few experiments conducted to evaluate the system performance. We show BER measurements for m-sequences of length 7 and 15. We also present the system performance as a function of the received power. We finally present a detailed power budget.

4.1 Experimental Set-up

The experimental set-up used to prove the concept of optical CDMA spectral amplitude encoding is shown in Fig. 4.1. The transmitter and receiver have been assembled as in Fig. 3.5 and 3.8, respectively.

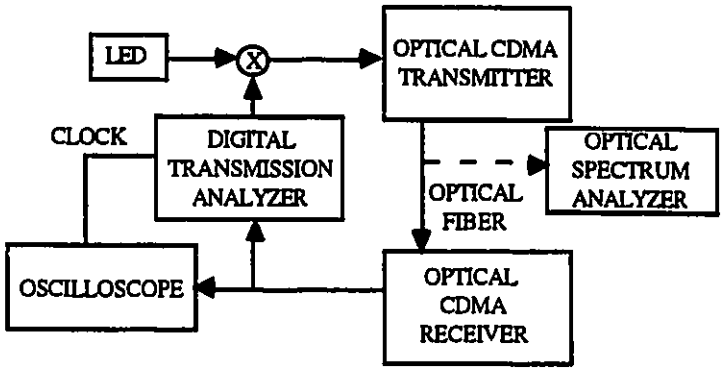

Fig. 4.1 Schematic diagram of the set-up used for the optical CDMA amplitude encoding experiment. The blocks "Optical CDMA Transmitter" and "Optical CDMA Receiver" were presented in Fig. 3.5 and 3.8, respectively.

Multi-mode fibers with 200/240 μm core/cladding diameters and 0.37 numerical aperture were used in the transmitter and in the point-to-point connection to the receiver. A

Multi-mode fibers with 200/240 μm core/cladding diameters and 0.37 numerical aperture were used in the transmitter and in the point-to-point connection to the receiver. A LED at 810 nm with a 3 dB spectral bandwidth of 50 nm and a maximum coupled power of 2 mW has been used, along with a driver for on-off keying modulation at 10 kbps and 20 kbps. The data stream coming from a digital transmission analyzer modulates the intensity of the LED. The optical signal is encoded in the transmitter and is coupled into the multi-mode fiber. After propagating through the fiber, the optical signal is decoded in the differential receiver and fed back to the digital transmission analyzer. The eye patterns were observed on a digital oscilloscope. The fiber exiting the transmitter was connected to an optical spectrum analyzer in order to measure the encoded spectrum.

Although we used a modest bit rate to demonstrate data transmission, the passive all-optical nature of the encoding technique allows transmission at much higher rates. Indeed, the electric signal format (e.g., rate, pulse shape and modulation format) is completely transparent to the way this optical switch/LAN operates [3,4]. Therefore, electric signals at higher bit rates can be used the same way as we use a low bit rate signal.

Aspheric lenses Melles Griot 01 LAG 025 with a plano back-surface and a focal length of $f = 79$ mm, diameter of $\phi = 84$ mm and $f/\phi = 0.94$ were used in both the encoder and the decoder for collimating and focusing. Aspheric lenses are very suitable for this application. Their focal length is much shorter than that of a spherical lens of equal diameter and identical spherical aberrations. The aspheric surface corrects the path of the severely aberrated marginal rays, reduces coma and spherical aberration and focuses more energy into a smaller area. Plano back-surface has the advantage of forming small focal spots.

The gratings used are in near Littrow configuration, i.e., the diffracted beam comes back close to its incident direction. Different wavelengths are separated and focused by the same lens onto different spots on an amplitude code mask. All gratings used in the encoder and decoder are metallized plane holographic gratings on reflection with a sinusoidal

groove shape and with a constant spacing of 1200 grooves/mm and a 50x50 mm aperture size. Those gratings feature one diffraction order and the zero order of the nondiffracted light and exhibit low stray light. They are optimized for the infra-red region (IR), 700-1400 nm, and in use with nonpolarized light with their maximum diffraction efficiency of approximately 65% at the Bragg angle.

A pair of small plano-convex lenses Newport KPX 076 of $f = 24.5$ mm and $\phi = 24.5$ mm in the differential receiver are used to collect the light and fill the diameter of the photodetectors. The n-type silicon p-i-n photodiodes used (C30810 from EG&G) have a 1 cm^2 circular photosensitive area and a responsivity of 0.5 A/W at 850 μm.

The mask patterns were generated on a computer and printed on transparencies with a laser printer. Experiments were conducted with masks representing m-sequences of length 7 and 15. The encoding was performed on the 3 dB bandwidth of the LED spectrum of 62 nm that was coupled back in the output fiber of the transmitter. Each chip of the mask pattern was of equal width : 1 mm for the 7 chip mask and 0.5 mm for the 15 chip case.

4.2 Bit-Error Rate Performance

4.2.1 7 Chip Mask

Fig. 4.2 shows the spectrum encoded with a 7 chip mask, as measured by an optical spectrum analyzer connected after the transmitter. The sequence of 0's and 1's represents the encoding m-sequence. Also shown is the corresponding mask pattern. The different portions of the spectrum clearly coincide with the 1's and 0's of the m-sequence. Drops in power correspond to the 0's. Even though quite acceptable, the sharpness of the edges of the spectrum is reduced by the optical spectral resolution and by the sharpness of the mask chips and their insufficient opacity. Aberrations are also present in the system, even if partially corrected by the lenses. However, masks with sharper edges and increased opacity are commercially available which we believe will improve the edges sharpness.

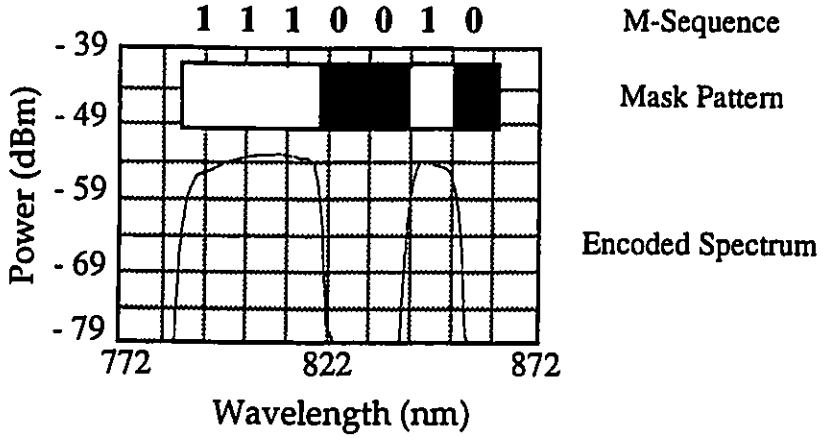

Fig. 4.2 Spectrum as encoded by a 7 chip mask. The corresponding m-sequence and mask pattern are also shown.

An important factor to assure user orthogonality is to achieve an acceptable extinction ratio. In Fig. 4.2, the encoded spectrum has an extinction ratio of 25 dB. Under these testing conditions, we obtained a measured bit error rate (BER) below 10^{-9} for bit rates of 10 kbps and 20 kbps.

Fig. 4.3 shows the eye patterns resulting from the optical signal received in each arm of the differential receiver. The top eye-pattern corresponds to the signal detected by the arm with the matching code, while the bottom one is associated with the complementary mask. The eye of the lower signal is closed, meaning that the complementary mask filters out the received signal very efficiently. In Fig. 4.3 (b), we can see the eye pattern recovered from the subtraction of the signals in Fig. 4.3 (a). It has a peak-to-peak amplitude of 5 Volts. The high noise level in Fig. 4.3 comes from the fact that very little light is detected by the photodiodes (a few nanowatts). Therefore, the current generated by the photodiode is extremely low (tens of nA), which requires a very large amplification for signal processing (a 1 MΩ resistor was necessary - see Fig. 4.7). The amplification and the subsequent electronic processing introduced a significant amount of thermal noise. A better signal recovery design can greatly improve the noise figure of the final output. However, one can still see a good eye opening, meaning that low error rates are achievable. A better electronic recovery system can be designed to improve the noise figure [48].

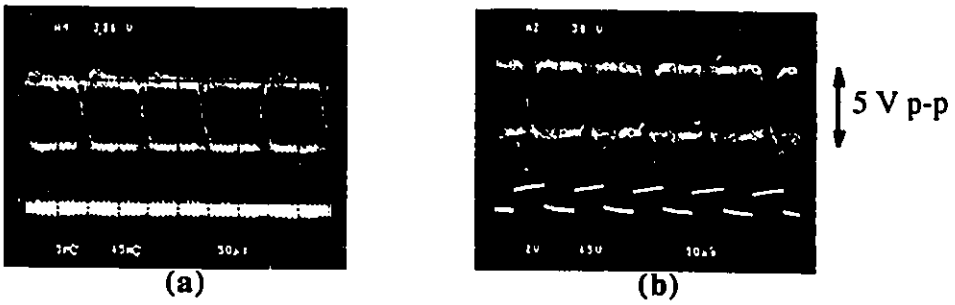

Fig. 4.3 Eye pattern measurements obtained with a 7 chip code. The top eye pattern in (a) corresponds to the signal detected by the matching mask, while the bottom eye pattern corresponds to the signal detected after the complementary mask. Fig (b) shows the resulting eye pattern. The bottom signal in (b) is the system clock.

A complete proof-of-concept must verify that data sent to an intended user is received only by this user. To test the processing gain, a different user was simulated in the transmitter by shifting the code by two bits relative to those in the receiver (Fig. 4.4). The recovered signal had a closed eye pattern, meaning the signal remained undetected.

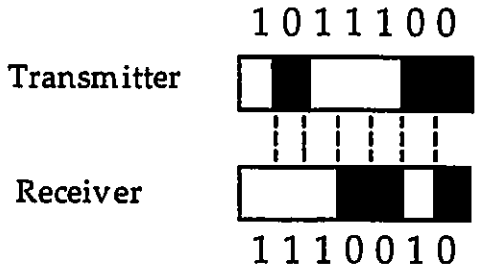

Fig. 4.4 Testing of the processing gain. The code in the transmitter was shifted by two chips relative to those in the receiver.

Orthogonality between users having adjacent address codes was not obtained. The loss of orthogonality is due to the insufficient edges sharpness of the encoded spectrum. For a one bit shift in the transmitter, we obtained an eye pattern with a 1.5 V p-p opening, that is 30% of the peak-to-peak amplitude for matching masks in the encoder and decoder. Orthogonality with the complementary code might still be achieved, but only if one user is transmitting data in the channel. However, there is a 1 nm uncertainty associated with the mask alignment method. It was obtained by observing of the spectrum with an optical spectrum analyzer. The effect of insufficient processing gain loss is explained in the next section.

4.2.2 15-Chip Mask

Similar measurements were made with an encoding mask of 15 bits. The encoded spectrum is shown in Fig. 4.5. The extinction ratio is much lower than for the 7 chip encoded spectrum, approximately 15 dB. This low extinction ratio can be improved by a few dB with the use of more opaque masks. However, a BER below 10^{-9} was measured at 10 kbps. The code length is much shorter than the theoretical limit of 31 as computed in chapter 3. However, this limit was evaluated neglecting the effect of spherical aberrations, which influence the true maximum system resolution.

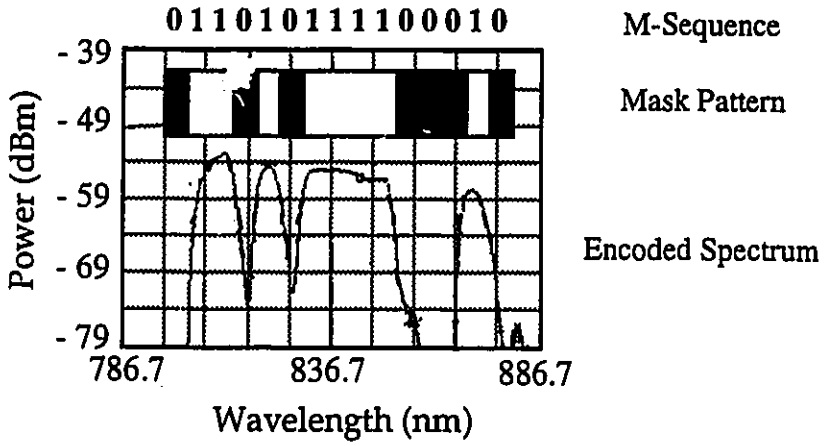

Fig. 4.5 Spectrum as encoded by a 15 chip mask, with corresponding m-sequence and mask pattern.

The low extinction ratio resulted in a loss in the processing gain, as depicted in Fig. 4.6. The eye patterns in (a) and (b) are respectively, the one recovered in the arm with the matching mask, the one from the complementary mask branch, and the resulting eye pattern. We were still able to obtain a satisfactory eye opening with the low extinction ratio. The problem arises for an unfriendly user. The eye-pattern in Fig. 4.6 (c) was obtained when the code in the transmitter was shifted by one bit with reference to the code in the receiver. The eye-pattern has now an opening of 2 Volts peak-to-peak, when a closed eye pattern is expected. The eye opening is attributed to the low extinction ratio, to the edge sharpness of the encoded spectrum, and to mask misalignments.

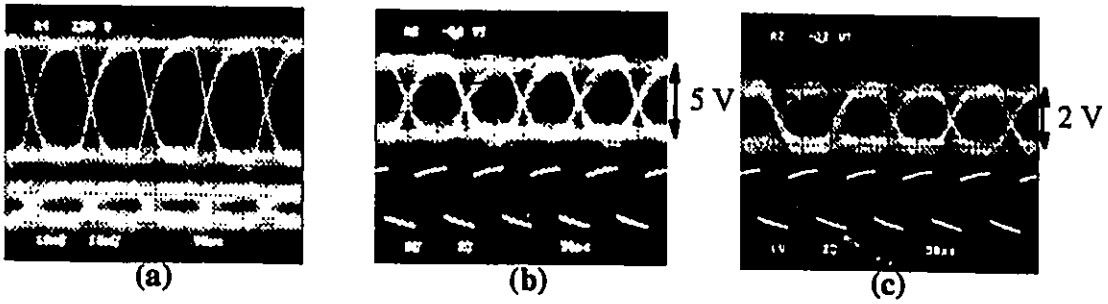

Fig. 4.6 Eye pattern measurements obtained with a 15 chip code. In (a) and (b), the masks in the transceivers are aligned. The top eye pattern in (a) corresponds to the signal detected by the matching mask, while the bottom eye pattern corresponds to the signal detected after the complementary mask. Fig (b) shows the resulting eye pattern. It has an eye opening of 5 V p-p. The eye pattern in (c) was obtained with a 1-bit mismatch between the codes in the transceivers. It has an eye opening 2 V p-p.

This case implies an insufficient processing gain. If many users send data simultaneously, the different signals will add up in the network. Therefore, an unintended user might receive data even if nothing was sent to him. Let's take the present case as an example. Suppose user A is sending data, not destined to user C. Also suppose a threshold decision level of 2.5 V. We neglect the near-far effect. At the user C receiver, the processing of the data from user A will give rise to an eye pattern of 2 volts peak to peak, which is under the decision level, therefore it will remain undetected. If data from user B is broadcasted through the network, once again the optical processing will give rise to a 2 volts peak-to-peak eye pattern. However, if users A and B decide to send data simultaneously and since all the users share the same transmission medium, the resulting eye pattern at receiver C will have a maximum eye opening of 4 volts peak-to-peak, which will be above the 2.5 V threshold level. Therefore, user C might receive some data. However, the use of better masks will increase the extinction ratio, and the receiver will be able to reject interfering signals.

Insufficient processing gain was also experimented by Iversen et al. [24], with the acousto-optic filtering approach. They felt necessary to reject many of the codewords in a set, because of insufficient processing gain between two adjacent codewords. The extinction ratio achievable with commercially available integrated acousto-optics filters is at

best 11 dB [47], for only one narrowband filter. The filtering approach requires many filters cascaded, therefore, the losses are accumulated and because of radio-frequency (RF) interference in the device, the overall extinction ratio will be a lot less than 11 dB. The filtering approach, although attractive for reasons of simplicity and integration, experiences the same problem of insufficient processing gain.

4.3 BER vs Received Power

An experiment was conducted at 20 kbps to evaluate the system performance according to different levels of received power by placing optical attenuators in the transmitter. The total amplitude of the eye pattern from the matching mask arm was first measured with an oscilloscope. From these measurements, we computed the corresponding optical power with the following equation:

$$I = \mathcal{R}P_o = \frac{V}{\mathrm{R}} \quad \Rightarrow \quad P_o = \frac{V}{\mathcal{R}\mathrm{R}} \tag{4.1}$$

where I is the photocurrent in A, $\mathcal{R}$ the photodiode responsivity in A/W, P_o the received optical power in W, V the voltage measured on the oscilloscope in Volts and R a resistor. The different parameters appearing in (4.1) are shown on Fig. 4.7, which represents the optical power detection and first amplification stages at the receiver. The results are plotted in Fig. 4.8.

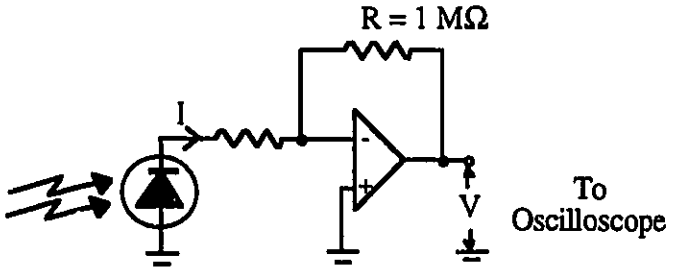

Fig. 4.7 Electrical parameters appearing in the computation of P_O.

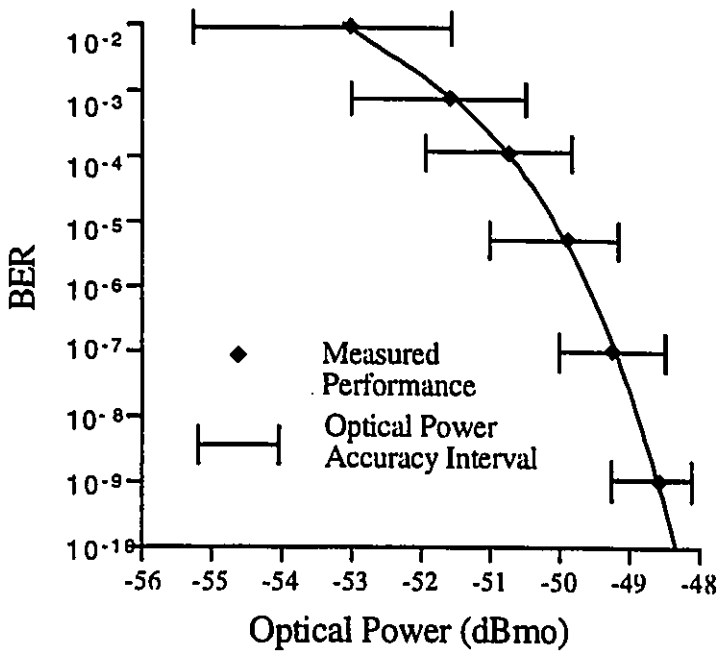

Fig. 4.8 Curve of Bit-Error Rate measurements as a function of Mean Optical Power detected in the arm with the matching mask.

It was impossible to measure the exact noise level with the available equipment because of the low bit rate. However, the noise level was fixed for all the measurements. Therefore, the curve in Fig. 4.8 represents the performance as a function of SNR. Since the detected power was so close to the detection limit of the photodiode, a resistor of 1 MΩ was necessary to perform signal amplification for further processing. The large amplification introduced an enormous level of thermal noise which was comparable to the signal level. This explains the large accuracy intervals on Fig. 4.8. The system performance can be greatly improve with an optimized detection stage. The interested reader may refer to [48]. However, even with non-optimized electronics, low BERs measurements were achieved. As seen from Fig. 4.8, the system behaves normally, that is increasing BER with decreasing signal power. Also, no error rate saturation floor was noticed.

4.4 Power Budget

A power budget of the proposed system was evaluated both theoretically and experimentally. The theoretical losses were evaluated according to the data specifications on each component. The grating efficiency at 830 nm is approximately 65% for each grating. The ratio of 1's in an m-sequence of length N is $\frac{N+1}{2N}$. As N increases, almost half the light is blocked. We therefore estimated a 3 dB mask loss. The losses for the lenses account for a 6% reflection loss after each passage, that is four passages all together. The coupling efficiency was evaluated by the computer simulation described in Section 3.3.4.

The experimental losses in the transmitter and receiver were evaluated by computing the difference between the input and output powers of each transceiver. At the transmitter, we defined the input power as the power launched in the 3 dB bandwidth of 62 nm coupled in the second fiber. A value of -22.16 dBm was measured with an optical spectrum analyzer. The output power of the transmitter is the power measured in the encoded spectrum. For the case in Fig. 4.2, we observed a value of -41.3 dBm. The input power at the receiver is approximately the same as the output power of the transmitter, since the transceivers were connected by a 2 meters fiber cable. The output power at the receiver was derived from the photodetector current, as in Section 4.3. We computed a detected output power of -48.5 dBm. The theoretical and experimental losses are listed in Table 4.1.

We computed a theoretical loss of -13.81 dB in the transmitter, compared to an observed experimental loss of -19.14 dB. The results are in agreement. The extra losses can be easily explained by misalignment of the gratings. The efficiency decreases when the incident beam does not hit the grating under its optimum incident angle. Because of bulky experimental equipment, the grating had to be tilted a little in order to couple light in the output fiber. We estimated a grating efficiency of 50% for each grating for the operating wavelength. We also estimated 1 dB loss due to light scattering at the encoding mask. Another extra 2 dB loss was attributed to the coupling losses.

	Theoretical losses (dB)	Experimental losses (dB)
TRANSMITTER:		
Gratings	-3.74	-6
Mask	-3	-4
Lenses	-1.07	-1.14
Coupling losses	-6	-8
Transmitter Losses	**-13.81**	**-19.14**
RECEIVER:		
Lenses	-0.54	-0.54
Grating	-2.22	-2.39
Beam Splitter	-3	-3
Matching Mask	0	-1
Collecting Lens	-0.27	-0.27
Receiver Losses	**-6.03**	**-7.2**
TOTAL LOSSES	**-19.84**	**-26.34**

Table 4.1 Theoretical and Experimental Optical Power Losses in the proposed system.

Because of the great reduction of optical components, the losses in the receiver are much less severe than in the transmitter. We computed a theoretical loss of -6.03 dB, compared to the -7.2 dB loss measured. The extra losses are again attributed to grating misalignments and mask scattering. The grating misalignment loss is less severe than in the transmitter because the light is incident onto a large area photodetector. Therefore, the grating does not have to be tilted as in the transmitter.

A significant portion of the loss can be attributed to mask misalignment. The alignment procedure relied on the eye opening observed on the oscilloscope. For the matching mask, one is looking for a maximum eye opening, while a minimum is desired for the complementary mask. For the 7 chip case, the alignment was easily obtained. However, as the codes get longer, many local maxima and minima can occur when aligning

the masks. Therefore, one has to test the system with BER measurements to verify the masks alignment. The most reliable method would be to collect all the light after the mask and measure it with an optical spectrum analyzer. However, as seen in Section 3.3.4, we are not able to focus all the light in a spot smaller than the fiber core, therefore making it impossible to measure it with a spectrum analyzer. Another possible solution would be to align the masks with a power detector.

As previously mentioned, optical CDMA is a power-limited system. This can be easily observed from Table 4.1, where we computed theoretical losses of almost -20 dB in the transceivers only. This does not take into account the splitting losses coming from the broadcasting of the signal by a star coupler. These losses are proportional to $10\log N$, where N is the number of users or the m-sequence length. For $N = 255$, the computed losses are -24 dB. Another factor to consider is the distance between two users. The further away two users are, the weaker the signal will be. Multi-mode fibers at 800 nm have an attenuation factor in the order of 5 dB/km [28]. If one could have a source powerful enough to overcome the losses, the problem would be solved. Superluminescent diodes are a possible solution. Some commercially available SLDs promise 0.6 mW out of a single-mode fiber [49]. Therefore, one can expect powers in the tens of milliwatts if coupled to a multi-mode fiber.

The transceivers high losses are however comparable to the numbers found in the literature concerning integrated spectrographs [35,36]. In [36], losses of approximately 16 dB have been reported. In [35], high insertion losses of 10.1 dB are experienced, however leading to an extinction ratio of 15 to 20 dB.

Chapter 5

Concluding Remarks and Suggestions for Further Study

In this thesis, a proof-of-concept demonstration of a new optical Code-Division-Multiple Access (CDMA) system was reported. This system is based on spectral amplitude encoding of noncoherent broadband sources such as LEDs or SLDs. Its advantages include the use of low-cost optical sources, and simple direct detection receivers. Compared to conventional time-encoded CDMA systems, the spreading gain of frequency-encoded CDMA systems is independent of the data rate, therefore individual users can operate asynchronously at data rates compatible with available electronic devices. However, spectral encoding CDMA is limited to LAN or switching applications, because of the dispersion problem associated with the propagation of broadband optical pulses and the limited modulation achievable with LEDs

In Chapter 2, we briefly surveyed current trends in optical CDMA research. The systems were classified according to the encoding domain, time, space or frequency. They were also classified according to the type of processing performed, i.e. coherent or incoherent. All time-encoded systems suffer from the same limitation of spreading gain. As data rates increase, the current electronics will not be able to process time-encoded CDMA signals because of their limited speed. Hybrid systems allow a better network bandwidth efficiency, but are very difficult to work with. They require simultaneous synchronism over many channels, whether those channels are different wavelength or spatial channels. We presented WDM spectral slicing because of its similarities with the optical CDMA

system presented in this thesis. Compared to spectral slicing for WDM applications, more power is available for CDMA encoding since it is performed over all the slots. However, WDM has the advantage of being routed throughout the network, and for that reason does not suffer from the splitting losses associated with the broadcasting of CDMA encoded pulses.

The optical CDMA system under study in this thesis was extensively explained in Chapter 3. The encoding and decoding principles rely upon the crosscorrelation properties exhibited by the set of signals used to distinguish subscribers, m-sequences or Hadamard codes. Other codes need to be investigated, such as Gold codes or Kasami codes. A perfect code for this application would be one that exhibits extremely low correlation between two different code words from the set. As the experiment showed, it is very difficult to align the masks at the receiver so that they exactly match the one at the transmitter. Therefore, an ideal code would require crosscorrelation properties such that slightly misaligned masks could still lead to good signal recovery or rejection.

As seen in Section 3.2.2, the theory of Fourier optics is not required to explain the encoding and decoding principles of spectral amplitude encoding. A distinction between phase encoding [22] and amplitude encoding was demonstrated. In the former case, it was shown that Fourier transform and inverse Fourier transforms have to be performed on the coded signals in order to recover the transmitted pulses. It is not the case for amplitude encoding, since the phase factor associated with propagation will always disappear, regardless of the distance between the gratings and the lenses in Fig. 3.3. An extensive system representation, in terms of Fourier optics, remains to be done. As mentioned in the same section, coherent encoding can be performed on phase, amplitude or on both. A new coherent encoding technique could therefore rely on simultaneous manipulations of phase and amplitude. If one is able to combine the binary coherent encoding proposed by Weiner et al. [22], and the binary noncoherent encoding depicted in this thesis, a ternary address

code could be accommodated by manipulating the phase of the unfiltered spectral components. Obviously, this technique would require the use of ultrashort pulses

Since exact Fourier transform was not necessary to recover data for this incoherent system, we were able to use a more compact configuration than what was originally proposed by our group. The next logical step is to integrate this system. We designed a transmitter and receiver with Littrow mounting. A single lens serves the double purpose of beam collimation and focusing. This grating configuration is very similar to another type of diffracting element called concave grating. Such devices have widely been reported in integrated spectrograph applications [36,37]. Spectrographs are instruments in which the whole spectrum is detected on an image detector or photodiodes array. By replacing the photodetectors by a reflective amplitude mask, a spectrograph can be turned into an optical CDMA encoder. Demonstrated on silica and semiconductor, the spectrographs reported in [36,37] use a concave grating. Such a grating not only disperses light into a spectrum, but also focuses it into a sharp image, without the use of any lens or external collimating device. This configuration is simpler than Littrow configuration, because no lenses are required to perform the focusing. It would be interesting to demonstrate spectral amplitude encoding with such gratings. The mask design should prove to be quite a challenge, though. Because of the spherical shape of the grating, every single chip of the mask would have to be tilted so that the unfiltered wavelengths are collimated back into the output optical fiber connected to the star coupler. Therefore, it will be a lot simpler to repeat the experiments with a Littrow mounting configuration and one reflective mask, as proposed in Chapter 3. Even though this design requires a lens, the number of optical components are reduced, compared to the configuration used for the experiment. The one-lens grating apparatus is depicted in Fig. 3.6. In this situation, a simpler plane reflective mask could be used.

A major contribution of this thesis lies in the simplification of the receiver design. The number of optical components was ultimately reduced from four gratings and lenses to

only one encoding apparatus. We suggest to split the signal after the different spectral components are angularly dispersed. Therefore, a beam splitter was placed right after the focusing lens. However, because of the location of the beam splitter, one has to take extra precautions when aligning the system. The beam splitter can be easily placed in the path of the incident light beam, which would alter the focused spectrums composition. The large area photodetectors necessary to collect all the light can also be a problem. As the area of a photodetecting surface increases, its capacitance increases as well. This results in an increase of the time constant of the detection system, which ultimately results in a degraded frequency response and a reduction of electrical bandwidth. Lenses with longer focal length could be placed before the detector, to reduce the area of the spot diagram in Fig. 3.14 (c). This would allows the system to operate at faster transmission rates.

In Section 3.3, we reported how the optical characteristics of the transceivers affect the system multi-access capacity. The system spectral resolution determines the minimum wavelength slot width, therefore the maximum number of users this system can accommodate. For our system in a diffraction limited situation, up to 3100 users could be theoretically accommodated. However, this is far from being practical. First, the splitting losses associated with the signal redistribution to the 3100 users would be enormous. Also, a diffraction limited case implies the use of single-mode fibers, which are limited by the so-called "excess-noise" [29] and which have very low coupling efficiency with LEDs. Consequently, it would be more realistic to use multi-mode fibers. High modal dispersion limits multi-mode fiber based systems to LAN applications and switches. Hence, spectral amplitude encoding could be an excellent candidate for switching applications, for example in ultrafast ATM networks [5].

The ray tracing technique applied to the CDMA encoding and decoding apparatus demonstrated how the optical aberrations affect the shape of the spectrum to be filtered. These aberrations emerge from the off-axis operation and large lens aperture. The spot diagrams in Fig. 3.14 indicate that even in the best case, the chosen Littrow configuration

imposes a spatial overlapping of the spectral components, as well as important coupling losses. All of these can be improved by the use of lenses with longer focal length, at the expense of system compactness. Therefore, when designing the transceivers, a compromise has to be reached between power throughput, optical spectral resolution (related to system capacity), aberrations and compactness.

We provided a few solutions for possible problems that can arise when implementing spectral amplitude encoding optical CDMA as a system. First, the LED spectrum might not be flat. If that is the case, the codes will appear as being multilevel, and user orthogonality will be lost. For the experiment, we concentrated on the simplest and more practical solution to limit the encoding to the 3 dB bandwidth. Also, the amplitude masks should be programmable. At present, SLMs with fast programming time but low contrast ratio have been reported.

The performance of the proposed CDMA system was experimentally obtained, and the results are reported in Chapter 4. We measured an extinction ratio of at least 25 dB for a 7-chip encoding mask, and 15 dB for a 15-chip encoding mask. We believe that masks with better contrast and sharper edges will increase the extinction ratio by a few dBs. BER values below 10^{-9} were measured for both cases, at rates of 10 kbps and 20 kbps. Although we used modest bit rates, the passive all-optical nature of the encoding technique allows transmission of up to hundreds Mbps. The low bit rate is explained by the electronic circuit design of the signal recovery system at the receiver. Even though the purpose of this thesis was to transmit data using spectral amplitude encoding, the system needs to be characterized at higher bit rates. Measurements of BER vs received power showed that the system does behave normally, i.e., improved performance with increased signal power.

The eye patterns reported in Chapter 4 show that, for matched transmitter and receiver, the receiver has good rejection capabilities. The signal remains undetected by a user if its code is more than 1-bit shifted relative to that in the transmitter. However, the

rejection capability of the receiver is not satisfactory for a 1-bit shift, for both the 7 and 15 chip m-sequences. Here we observe the consequences that optical aberrations can bring to the encoding and decoding procedure. An effort should be made in order to reduce the spherical aberrations in the system. An insufficient processing gain was also experienced by Iversen et al., with acousto-optic tunable filters [24]. They felt necessary to reject half of the code words available in an m-sequence set. The processing gain should be experimentally characterized, by simulating many simultaneous users and measuring the BER as a function of received power.

The main limitation of optical CDMA by spectral encoding is most probably associated with optical losses, which are inherent to the encoding technique. In Section 4.5, a power budget of the experimental system was evaluated, both theoretically and experimentally. We measured losses of -26 dB compared to the -20 dB losses computed theoretically, not counting the propagation losses and splitting losses arising from signal broadcasting. The main source of losses in the transceivers is the limited efficiency of diffraction gratings for non-polarized light. Also, because of off-axis operation, more than 8 dB of losses are experienced when coupling light to the second fiber in the transmitter. An important effort should be made in encoder/decoder design in order to collect the most light possible. A powerful enough source, e.g., SLD, could however overcome the losses.

APPENDIX

Detailed Electronic Circuits for LED Driver and Signal Recovery System

A.1 LED Driver

LED: High-Performance LED 1A272 from ABB HAFO

Peak wavelength 810 nm

Spectral width (FWHM) 50 nm

Maximum power coupled in 200/240 μm step-index fiber *NA* 0.37 = 2 mW

All these characteristics are for an operating voltage of 100 mA and a forward voltage of 2.4 V

Transistor: MPQ2222

Typical h_{FE} (β) 100 to 300 (for I_c=150 mA and V_{CE}=10 V)

When the transistor is saturated, the LED is turned on and vice versa.

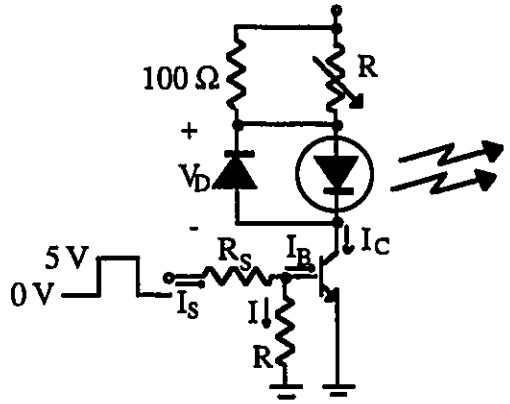

$V_{CC} = 5$ V

$V_{BE} = 0.7$ V

$(R)_{MAX} = 100\ \Omega$

$R_S = 1800\ \Omega$

$R = 10$ kΩ

$I = V_{BE}/R = (0.7\text{ V})/(10\text{ k}\Omega) = 0.7\ \mu\text{A}$

$$I_S = \frac{V_S - V_{BE}}{R_S} = \frac{(5\text{ V}) - (0.7\text{ V})}{1800\text{ W}} = 2.4\ \mu\text{A}$$

$I_B = I_S + I = I_S$

$I_c = \beta I_B$

$$I_c = \frac{V_{cc} - V_D}{R_c} = \frac{(5\text{ V}) - V_D}{(100\Omega)\|(R)}$$

The reverse-polarized diode is in the circuit just as a matter of protection for the LED.

A.2 First Amplification Stage

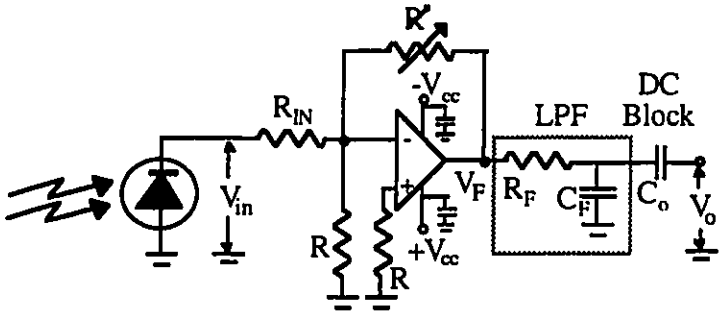

$|V_{cc}| = 12$ V $R_F = 270\ \Omega$

$R_{IN} = 18$ kΩ $C_F = 0.22\ \mu$F

$R = 10$ kΩ $C_o = 0.22\ \mu$F

$(R)_{MAX} = 1$ MΩ

$$V_F = -\frac{R}{R_{IN}} V_{IN} = RI_{IN}$$

$$\underline{\text{LPF}} : \ \mathrm{H}(f) = \frac{1}{1 + \mathrm{j}(f/f_c)}; \ f = (2\pi\tau)^{-1}; \ \tau = R_c F_c$$

It is preferable to decouple the DC power supply V_{CC} from the circuit with capacitors in order to avoid self-oscillation.

A.3 Subtraction and Second Amplification Stage

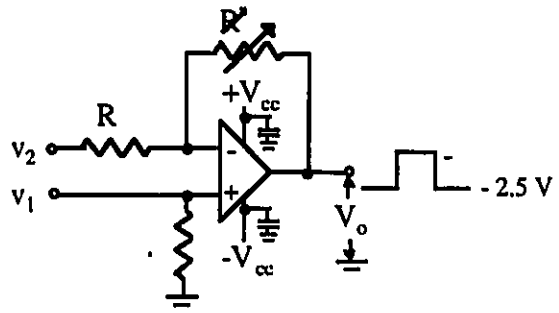

$|V_{cc}| = 12$ V

$R = 1$ kΩ

$(R)_{MAX} = 1$ MΩ

$$V_o = \frac{(R+R)}{R} V_1 - \frac{R}{R} V_2$$

$$= \frac{R}{R}(V_1 - V_2) \quad \text{for} \quad R >> R$$

A.4 Threshold and Decision Circuit

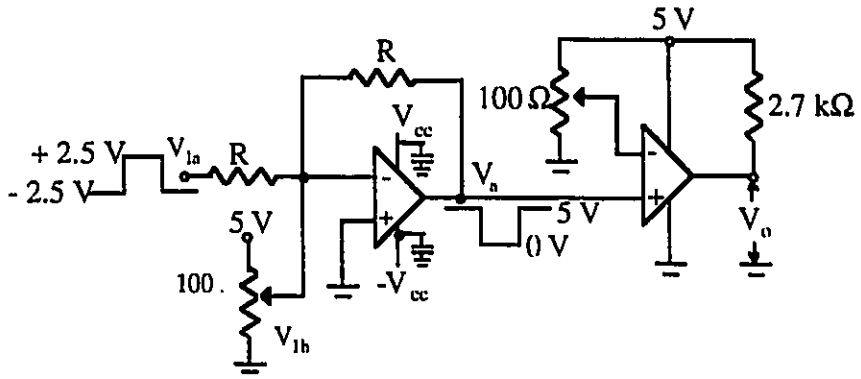

$R = 1\ \text{k}\Omega$

$|V_{cc}| = 12\ \text{V}$

$$1^{\text{st}}\ \text{stage}: \ V_a = -\frac{R}{R}V_{1a} - V_{1b} = -(V_{1a} + 2.5\ \text{V})$$

$$2^{\text{nd}}\ \text{stage}: \ V_o = A[(V_+) - (V_-)] = \begin{cases} 5\ \text{V} & \text{if } V_+ > V_- \\ 0\ \text{V} & \text{if } V_+ < V_- \end{cases}$$

where A is the open loop gain of the operational amplifier, V_+ is the incoming signal (0,5V), and V_- is the threshold (2.5 V).

A.5 TTL Driver

We have to match the output impedance of the circuit to that of the digital transmission analyzer, which operates under TTL level, that is (0,5 V) and input impedance of 75 Ω.

The value of R is set so as to saturate the transistor. When such is the case, then we have:

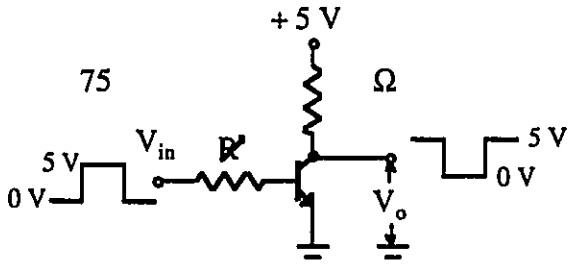

$(R)_{MAX} = 20\ \text{k}\Omega$

$V_{BE} = 0.7\ \text{V}$

$$I_c = \frac{V_{cc} - V_o}{R_c} \quad \text{and} \quad I_B = \frac{I_c}{\beta} = \frac{V_{cc}}{\beta R_c} = \frac{V_{in} - V_{BE}}{R}$$

$$V_o = V_{cc} - R_c I_c$$

References

[1] F. P. Kapron, D. B. Beck and R. D. Maurer. "Radiation Losses in Glass Optical Waveguides," Appl. Phys. Lett., vol. 17, pp. 423-425, Nov. 1980.

[2] T. Li, "The Impact of Optical Amplifiers on Long-Distance Lightwave Telecommunications," Proc. IEEE, vol. 81, no. 11, pp. 1568-1579, Nov. 1993.

[3] D. Zaccarin and M. Kavehrad, "An Optical CDMA System Based on Spectral Amplitude Encoding of LED," IEEE Photon. Technol. Lett., vol. 4, no. 4, pp. 479-482, April 1993.

[4] D. Zaccarin and M. Kavehrad, "Optical CDMA by Spectral Encoding of LED for Ultrafast ATM Switching," ICC'94, pp. 1369-1373.

[5] M. Kavehrad and D. Zaccarin, "Optical Code-Division-Multiplexed Systems Based on Spectral Encoding of Noncoherent Sources," J. Lightw. Techn., vol. 13, no. 3, pp. 534-545, March 1995.

[6] L. Adam, E. Simova and M. Kavehrad, "Experimental Optical CDMA System Based on Spectral Amplitude Encoding of Noncoherent Broadband Sources", Proceedings Photonics East, SPIE vol. 2614, paper 2614-15, pp. 122-132, Philadelphia, October 1995.

[7] K. Iversen and D. Hampicke, "Comparison and Classification of All-Optical CDMA Systems for Future Telecommunication Networks," Proceedings Photonics East, SPIE vol. 2614, paper 2614-14, Philadelphia, October 1995.

[8] D. Zaccarin, "Novel Architectures and Multiplexing Strategies for Optical CDMA," Ph.D Thesis, University of Ottawa, 1994.

[9] F. R. K. Chung, J. A. Salehi and V. K. Wei, "Optical Orthogonal Codes: Design, Analysis, and Applications," IEEE Trans. Inform. Theory, vol. 35, no. 3, pp. 595-604, May 1989.

[10] S. V. Maric, Z. I. Kostic and E. L. Titlebaum, "A New Family of Optical Code Sequences for Use in Spread-Spectrum Fiber Optic Local Area Networks," IEEE Trans. Commun., vol. 41, no. 8, pp. 1217-1221, Aug. 1993.

[11] P. R. Prucnal, M. A. Santoro and T. R. Fan, "Spread Spectrum Fiber-Optic Local Area Network Using Optical Processing," J. Lightw. Techn., vol. LT-4, no. 5, pp. 547-554, May 1986.

[12] R. Petrovic and S. Holmes, "CDMA Techniques in Optical Fiber LANs," J. Opt. Comm., vol. 12, no. 3, pp. 101-106, 1991.

[13] J. A. Salehi, "Code Division Multiple-Access Techniques in Optical Fiber Networks - Part I: Fundamental Principles," IEEE Trans. Commun., vol. 37, no. 8, pp. 824-833, Aug. 1989.

[14] J. A. Salehi and C. A. Brackett, "Code Division Multiple-Access Techniques in Optical Fiber Networks - Part II: Systems Performance Analysis," IEEE Trans. Commun., vol. 37, no. 8, pp. 834-842, Aug. 1989.

[15] A. S. Holmes and R. R. A. Syms, "Switchable All-Optical and Decoding Using Optical Fibre Lattices," Optics Communications, vol. 86, no. 1, pp. 25-28, 1991.

[16] W. C. Kwong, P. R. Prucnal and Y.-L. Liu, "Ultrafast All-Optical Code-Division Multiple Access Networks," Proc. SPIE, Multigigabit Fiber Communications, vol. 1789, pp. 121-132, 1992.

[17] L. Nguyen, B. Aazhang and J. F. Young, "All-Optical CDMA with Bipolar Codes," Electron. Lett., vol. 31, no. 6, pp. 469-470, March 1995.

[18] S. Benedetto and G. Olmo, "Performance Evaluation of Coherent Optical Code Division Multiple Access," Electron. Lett., vol. 27, no. 22, pp. 2000-2002, Oct. 1991.

[19] D. D Sampson and D. A. Jackson, "Spread-Spectrum Optical Fiber Network Based on Pulsed Coherent Correlation," Electron. Lett., vol. 26, pp. 1550-1552, Sept. 1990.

[20] M. E. Marhic and Y. L. Chang, "Pulse Coding and Coherent Decoding in Fiber-Optic Ladder Networks," Electron. Lett., vol. 25, pp. 1535-1536, Oct. 1989.

[21] R. A. Griffin, D. D. Sampson and D. A. Jackson, "Demonstration of Data Transmission Using Coherent Correlation to Reconstruct a Coded Pulse Sequence," IEEE Photon. Technol. Lett., vol. 4, pp. 513-515, May 1992.

[22] A. M. Weiner, J. P. Heritage and J. A. Salehi, "Encoding and Decoding of Femtosecond Pulses," Opt. Lett., vol. 13, no. 4, p. 300-302, April 1988.

[23] X. S. Yao, J. Feinberg, R. Logan, and L. Maleki, "Limitations on Peak Pulse Power, Pulse Width, and Coding Mask Misalignment in a Fiber-Optic Code-Division Multiple Access System," J. Lightw. Technol., vol. 11, no. 5/6, pp. 836-846, May/June 1993.

[24] K. Iversen and O. Ziemann, "An All-Optical CDMA Communication Network by Spectral Encoding of LED Using Acousto-Optic Tunable Filters," Int. Symp. on Signals, Systems and Electronics (ISSSE'95), San Francisco, Paper FA3-4, Oct. 1995,

[25] K. Kitayama, "Novel Spatial Spread Spectrum Based Fiber Optic CDMA Networks for Image Transmission," IEEE J. Select. Areas Commun., vol. 12, no. 4, May 1994

[26] Y. Su, X. Chen, private communication.

[27] T. V. Higgins, "Light Speeds Communications,"" Laser Focus World, vol. 31, no. 8, pp. 67-74, Aug. 1995.

[28] G. Keiser, "Optical Fiber Communications," 2nd ed., McGraw-Hill, New York, 1991.

[29] E. D. J. Smith, P. T. Gough and D. P. Taylor, "Noise Limits of Optical Spectral-Encoding CDMA Systems," Electron. Lett., vol. 31, no. 17, pp. 1469-1470, Aug. 1995.

[30] P. P. Iannone, N. J. Frigo and T. E. Darcie, "WDM Passive-Optical-Network Architecture with Bidirectional Optical Spectral Slicing," OFC'95 Tech. Dig., pp. 51-53.

[31] J. S. Lee, Y. C. Chung and D. J. DiGiovanni, "Spectrum-Sliced Fiber Amplifier Light Source for Multichannel WDM Applications," IEEE Photon. Technol. Lett., vol. 5, no. 12, pp. 1458-1461, Dec. 1993.

[32] E. A. De Souza, M. C. Nuss, M. Zirngibl and C. H. Joyner, "Spectrally Sliced WDM Using a Single Femtosecond Source," OFC'95 Postdeadline, Paper PD16.

[33] E. Park, A. J. Mendez, and E. M. Garmire, "Temporal/Spatial Optical CDMA Networks-Design, Demonstration, and Comparison with Temporal Networks," IEEE Photon. Technol. Lett., vol. 4, no. 10, pp. 1160-1162, Oct. 1992.

[34] L. Tancevski, I. Andonovic, and J. Budin, "Secure Optical Network Architectures Utilizing Wavelength Hopping/Time Spreading Codes," IEEE Photon. Technol. Lett., vol. 7, no. 5, pp. 573-575, May 1995.

[35] L. Tancevski and I. Andonovic, "Wavelength Hopping/Time Spreading Code Division Multiple Access Systems," Electron. Lett., vol. 30, no. 17, pp. 1388-1390, Aug. 1994.

[36] P. C. Clemens, R. März, A. Reichelt and H. W. Schneider, "Flat-Field Spectrograph in SiO_2/Si," IEEE Photon. Technol. Lett., vol. 4, no. 8, pp. 886-888, 1992.

[37] J. B. D. Soole, A. Scherer, H. P. LeBlanc, N. C. Andreadakis, R. Bhat and M. A. Koza, "Monolithic InP/InGaAsP/InP Grating Spectrometer for the 1.48-1.56 μm Wavelength Range," Appl. Phys. Lett., vol. 58, no. 18, pp. 1949-1951, May 1991.

[38] D. V. Sarwate and M. B. Pursley, "Crosscorrelation Properties of Pseudorandom and Related Sequences," Proc. IEEE, vol. 68, no. 5, pp. 593-619, May 1980.

[39] J. G. Proakis, "Digital Communications," 2nd ed., McGraw Hill, New York, 1989.

[40] J. W. Goodman, "Introduction to Fourier Optics," 2nd ed., McGraw Hill, New York, 1985.

[41] M. C. Hutley, "Diffraction Gratings," Academic Press, London, 1982.

[42] M. Born and E. Wolfe, "Principles of Optics," 6th ed., Pergamon Press, Oxford, 1989.

[43] A. Nussbaum and R. A. Phillips, "Contemporary Optics for Scientists and Engineers," Prentice Hall, Englewoods Cliffs, N. J., 1976.

[44] G. Andersson et al., "Submicrosecond Electro-Optic Switching in the Liquid-Crystal Smectic A Phase: the Soft-Mode Ferroelectric Effect," Appl. Phys. Lett., vol. 51, pp. 640-642, 1987.

[45] A. M. Weiner, D. E. Leaird, J. S. Patel, and J. R. Wullert II, "Programmable Shaping of Femtosecond Optical Pulses by Use of 128-Element Liquid Crystal Phase Modulator," IEEE J. Quantum Electron., vol. 28, no. 4, pp. 908-920, April 1992.

[46] S. F. Su, R. Olshansky, G. Joyce, D. A. Smith and J. E. Baran, "Use of Acoustooptic Tunable Filters as Equalizers in WDM Lightwave Systems," Dig. OFC'92, paper ThC4, pp. 203-204.

[47] Acousto-Optic Tunable Filter Model 4511, New Focus, Inc., 1995 Catalog.

[48] B. L. Kasper, "Receiver Design," Chapter 18 of Optical Fiber Telecommunications II, edited by S. E. Miller and I. P. Kaminow, Academic Press, 1988.

[49] Data Specifications of Super-Luminescent Diode OE360S in OKI Electronic Components Catalog, 1995.